



NAVAL POSTGRADUATE SCHOOL

Monterey, California



DTIC
ELECTE
MAR 4 1993
S C D

THESIS

OPTIMIZATION TECHNIQUES FOR CONTACT
STRESS ANALYSIS

by

Eric S. McDonald

December, 1992

Thesis Advisor

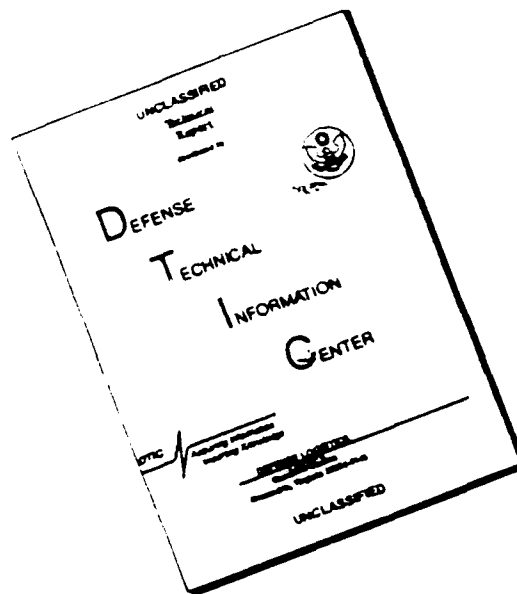
Y.W. Kwon

Approved for public release; distribution is unlimited.

93-04562



DISCLAIMER NOTICE



THIS DOCUMENT IS BEST
QUALITY AVAILABLE. THE COPY
FURNISHED TO DTIC CONTAINED
A SIGNIFICANT NUMBER OF
PAGES WHICH DO NOT
REPRODUCE LEGIBLY.

Unclassified

security classification of this page

REPORT DOCUMENTATION PAGE

1a Report Security Classification Unclassified			1b Restrictive Markings		
2a Security Classification Authority			3 Distribution Availability of Report		
2b Declassification Downgrading Schedule			Approved for public release; distribution is unlimited.		
4 Performing Organization Report Number(s)			5 Monitoring Organization Report Number(s)		
6a Name of Performing Organization Naval Postgraduate School		6b Office Symbol (if applicable) 34	7a Name of Monitoring Organization Naval Postgraduate School		
6c Address (city, state, and ZIP code) Monterey, CA 93943-5000			7b Address (city, state, and ZIP code) Monterey, CA 93943-5000		
8a Name of Funding Sponsoring Organization		8b Office Symbol (if applicable)	9 Procurement Instrument Identification Number		
8c Address (city, state, and ZIP code)			10 Source of Funding Numbers		
			Program Element No Project No Task No Work Unit Accession No		
11 Title (include security classification) OPTIMIZATION TECHNIQUES FOR CONTACT STRESS ANALYSIS					
12 Personal Author(s) Eric S. McDonald					
13a Type of Report Master's Thesis		13b Time Covered From To		14 Date of Report (year, month, day) December, 1992	
15 Page Count 90					
16 Supplementary Notation The views expressed in this thesis are those of the author and do not reflect the official policy or position of the Department of Defense or the U.S. Government.					
17 Cosati Codes			18 Subject Terms (continue on reverse if necessary and identify by block number)		
Field	Group	Subgroup	Contact Stress.Optimization.		
19 Abstract (continue on reverse if necessary and identify by block number)					
<p>The analysis of stresses induced by contact between two bodies is inherently difficult because the size of the contact zone is unknown and constantly changing throughout loading. To overcome these difficulties, two approximation methods have been developed to determine the magnitude of contact stresses using the Rayleigh-Ritz method and the finite element method. Numerical optimization methods are employed to solve the contact problem. The solution techniques are compared to known analytical solutions and shown to yield accurate results. An application of this approach to solving the contact problem is illustrated by examining the response of a clamped sandwich composite beam to low velocity impact. It was found that the maximum shear stress is insensitive to lamina thickness, however an increase in the contact layer thickness resulted in a reduction in interfacial shear stress. In addition, it was noted that a nonlinear bending stress distribution in the contact layer intensified as the thickness of this layer increased. This phenomenon was found to be localized to the region of contact. Finally, it was found that the compressive transverse normal stresses increased as the thickness of the contact lamina increased.</p>					
20 Distribution Availability of Abstract			21 Abstract Security Classification		
<input checked="" type="checkbox"/> unclassified unlimited <input type="checkbox"/> same as report <input type="checkbox"/> DTIC users			Unclassified		
22a Name of Responsible Individual Y.W. Kwon			22b Telephone (include Area code) (408) 646-2033		22c Office Symbol 54Ss

DD FORM 1473.84 MAR

83 APR edition may be used until exhausted
All other editions are obsolete

security classification of this page

Unclassified

Approved for public release; distribution is unlimited.

Optimization Techniques for Contact Stress Analysis

by

Eric S. McDonald
Lieutenant, United States Navy
B.S., U.S. Merchant Marine Academy, 1986

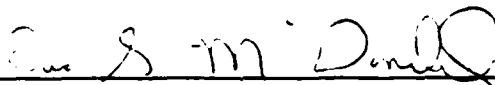
Submitted in partial fulfillment of the
requirements for the degrees of

MASTER OF SCIENCE IN MECHANICAL ENGINEERING
and
MECHANICAL ENGINEER

from the

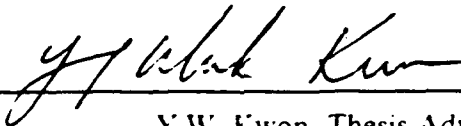
NAVAL POSTGRADUATE SCHOOL
December, 1992

Author:



Eric S. McDonald

Approved by:

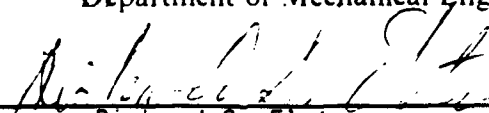


Y.W. Kwon, Thesis Advisor



Matthew D. Kelleher, Chairman.

Department of Mechanical Engineering



Richard S. Elster
Dean of Instruction

ABSTRACT

The analysis of stresses induced by contact between two bodies is inherently difficult because the size of the contact zone is unknown and constantly changing throughout loading. To overcome these difficulties, two approximation methods have been developed to determine the magnitude of contact stresses using the Rayleigh-Ritz method and the finite element method. Numerical optimization methods are employed to solve the contact problem. The solution techniques are compared to known analytical solutions and shown to yield accurate results. An application of this approach to solving the contact problem is illustrated by examining the response of a clamped sandwich composite beam to low velocity impact. It was found that the maximum shear stress is insensitive to lamina thickness, however an increase in the contact layer thickness resulted in a reduction in interfacial shear stress. In addition, it was noted that a nonlinear bending stress distribution in the contact layer intensified as the thickness of this layer increased. This phenomenon was found to be localized to the region of contact. Finally, it was found that the compressive transverse normal stresses increased as the thickness of the contact lamina increased.

REPRODUCTION OF THIS DOCUMENT IS UNLIMITED

Accession For	
NTIS CRA&I	<input checked="" type="checkbox"/>
DTIC TAB	<input type="checkbox"/>
Unannounced	<input type="checkbox"/>
Justification	
By _____	
Distribution /	
Availability Codes	
Dist	Avail and/or Special
A-1	

TABLE OF CONTENTS

I. INTRODUCTION	1
A. MOTIVATION	1
B. LITERATURE SURVEY	2
II. FORMULATION OF THE CONTACT PROBLEM	5
A. PRINCIPLE OF MINIMUM TOTAL POTENTIAL ENERGY	5
B. CONTACT PROBLEM DESCRIPTION	6
C. NUMERICAL OPTIMIZATION	8
1. Optimization Fundamentals	8
2. Augmented Lagrange Multiplier Method	13
3. Optimizer and One-Dimensional Search	14
4. Convergence	15
III. APPROXIMATE SOLUTION TECHNIQUES	16
A. RAYLEIGH-RITZ APPROACH	16
1. Background	16
2. Application of the Rayleigh-Ritz Method to the Contact Problem.	17
3. Trial Function Selection	17
B. FINITE ELEMENT APPROACH	22
1. Total Potential Derivation	22
2. Optimization and Static Condensation	26
IV. RESULTS AND DISCUSSION	30
A. PROCEDURE VALIDATIONS	30
1. Rayleigh-Ritz Method Results	30
2. Finite Element Method Results	35
a. Two Thin Plates in Contact	35
b. Roller-Foundation Contact Problem	39
B. APPLICATION	43
V. CONCLUSIONS AND RECOMMENDATIONS	76

A. RAYLEIGH-RITZ APPROACH	76
B. FINITE ELEMENT APPROACH	77
C. COMMENTS ON OPTIMIZATION	77
D. SANDWICH COMPOSITE MATERIAL STUDY	78
E. RECOMMENDATIONS FOR FURTHER STUDY	78
REFERENCES	79
INITIAL DISTRIBUTION LIST	81

LIST OF TABLES

Table 1.	RAYLEIGH-RITZ RESULTS AT CONTACT POINT	32
Table 2.	FINITE ELEMENT RESULTS: TWO PLATES IN CONTACT	39
Table 3.	COMPARISON OF STRESSES NEAR THE POINT OF CONTACT	43

LIST OF FIGURES

Figure 1.	Roller-foundation assembly	7
Figure 2.	Contact zone cross section	7
Figure 3.	Analytical solutions for σ_y and σ_x	9
Figure 4.	Deformed contact zone	10
Figure 5.	Unconstrained minimization	11
Figure 6.	Constrained minimization	12
Figure 7.	Rayleigh-Ritz method applied to contact problem	18
Figure 8.	Contact zone	19
Figure 9.	Finite element method applied to contact problem	29
Figure 10.	Comparison of σ_y in a roller contact problem	33
Figure 11.	Comparison of σ_x in a roller contact problem	34
Figure 12.	Stress contour of σ_y from Rayleigh-Ritz method	35
Figure 13.	Stress contour of σ_x from Rayleigh-Ritz method	36
Figure 14.	Strain contour of ϵ_y from Rayleigh-Ritz method	37
Figure 15.	Strain Contour ϵ_x from Rayleigh-Ritz method	38
Figure 16.	Two thin plates in contact	39
Figure 17.	Finite element mesh for two plates in contact	40
Figure 18.	Finite element mesh for roller-foundation problem	41
Figure 19.	Deformed finite element solution: deformation magnified 100 times	44
Figure 20.	Analytical solution vs. approximate σ_y from finite element results	45
Figure 21.	Analytical solution vs. approximate σ_x from finite element results	46
Figure 22.	Stress contour σ_y from finite element results (increment 0.01 GPa)	47
Figure 23.	Stress contour σ_x from finite element results (increment 0.02 GPa)	48
Figure 24.	Strain contour ϵ_y from finite element results (increment 0.000035)	49
Figure 25.	Strain contour ϵ_x from finite element results (increment 0.00001)	50
Figure 26.	Clamped composite beam	51
Figure 27.	Finite element mesh for clamped beam model	52
Figure 28.	Determination of nodal contact	55
Figure 29.	Loaded beam: deformation magnified 100 times	56
Figure 30.	Stress contour: τ_{xy} for clamped beam model	57
Figure 31.	Stress contour: σ_x for clamped beam model	58

Figure 32. Stress contour: σ_y for clamped beam model (In region of contact)	59
Figure 33. Stress distribution: τ_{xy} for 0(3)-ISO(10)-0(3) laminate	60
Figure 34. Stress distribution: τ_{xy} for 0(4)-ISO(8)-0(4) laminate	61
Figure 35. Stress distribution: τ_{xy} for 0(5)-ISO(6)-0(5) laminate	62
Figure 36. Stress distribution: σ_y for 0(3)-ISO(10)-0(3) laminate	63
Figure 37. Stress distribution: σ_y for 0(4)-ISO(8)-0(4) laminate	64
Figure 38. Stress distribution: σ_y for 0(5)-ISO(6)-0(5) laminate	65
Figure 39. Stress distribution: σ_x for 0(3)-ISO(10)-0(3) laminate	66
Figure 40. Stress distribution: σ_x for 0(4)-ISO(8)-0(4) laminate	67
Figure 41. Stress distribution: σ_x for 0(5)-ISO(6)-0(5) laminate	68
Figure 42. Stress distribution: σ_x for 0(5)-ISO(6)-0(5) laminate at cross section C	69
Figure 43. Stress distribution: τ_{xy} for 0(3)-ISO(6)-0(7) laminate	70
Figure 44. Stress distribution: τ_{xy} for 0(8)-ISO(6)-0(2) laminate	71
Figure 45. Stress distribution: σ_y for 0(3)-ISO(6)-0(7) laminate	72
Figure 46. Stress distribution: σ_y for 0(8)-ISO(6)-0(2) laminate	73
Figure 47. Stress distribution: σ_x for 0(3)-ISO(6)-0(7) laminate	74
Figure 48. Stress distribution: σ_x for 0(8)-ISO(6)-0(2) laminate	75

I. INTRODUCTION

A. MOTIVATION

Contact stresses occur when two bodies exert forces over limited contact regions. Examples of contact stress include meshing gear teeth, cam shaft and pushrod contact, rollers in plate forming operations, roller and ball bearings in contact with races, shaft and journal bearing contact, and plate-pin connections.

Contact zones can be point, line, or surface in geometry. Because of the limited contact zone, the local stresses can be sufficiently high to be of major concern to the designer. Consequently, a thorough understanding of this phenomenon is essential. The first successful analytical solution to the contact problem between two spheres was solved in the late 19th century by Hertz. His solution can only be applied to simple geometries such as spheres, cylinders, and flat plates. Because of these limitations, alternate solution techniques were needed to accommodate more complex geometries and boundary conditions.

Unfortunately, the contact problem is difficult to study. The most significant difficulty is that the size of the contact zone is unknown and constantly changing throughout loading. Solutions are obtained by an iterative process. Consequently, the problem is highly nonlinear in its behavior. It is because of these difficulties that approximation and numerical methods are preferred in the solution of the contact problem. There are two general approaches used in the approximate techniques to solve the contact problem. One class applies specific iterative procedures to solve a nonlinear system of equations that represent the contact state. For example, the contact condition can be simulated by the introduction of additional coupling terms into the system of equations. The other class constructs a functional that includes the contact body constraint. The functional is then minimized using specific numerical programming techniques. Although these two classes use different procedures, there are several methods to incorporate the contact condition into the problem formulation that are common to both classes. Examples of these include the penalty method and the augmented Lagrange multiplier method. These methods specify the manner in which the contact boundary conditions are treated.

The objective of this study has two parts. First, two approximate solution techniques will be developed to obtain the solution of the general contact problem. These

techniques belong to the general class of methods that calculate a specific functional and then applies numerical programming methods to solve the contact problem. Second, these solution techniques will be verified by comparison with known analytical solutions. With the solution techniques verified, the methods will be applied to study an actual contact problem.

In order to accomplish the first objective, two models will be developed. The first method utilizes the Rayleigh-Ritz method to solve the contact problem. An assumed deformation field that satisfies the boundary conditions is carefully selected. Theory of elasticity relationships are applied to obtain an expression for the system's strain energy enabling calculation of the total potential. The minimization of the total potential energy enables the calculation of the contact stresses at any point in the body. The second model developed uses finite element analysis to accomplish the same objectives. The numerical minimization technique used in both cases is the augmented Lagrange multiplier method.

To accomplish the second objective, both methods will be verified by comparison with the Hertz solution of an infinitely long cylinder in contact with a flat plane. With verification completed, the contact stresses resulting from low velocity impact between objects and composite sandwich materials will be studied.

B. LITERATURE SURVEY

As discussed previously, there are two general approaches to solving the contact problem. One approach uses special procedures to solve a nonlinear system of equations. The other creates a functional that includes the contact boundary constraints. Although different, both approaches use similar mathematical methods to incorporate the contact condition into the problem formulation. Two of these methods are the Lagrange method and the penalty method. A detailed explanation of the method of employing the Lagrange method in nonlinear finite element analysis was discussed by Pian [Ref. 1]. Alternately, the penalty finite element method was used by Cheng [Ref. 2] to solve the multibody contact problem. The fundamental concept of the latter approach is the transformation of a constrained problem into an unconstrained one. This is done by penalizing (i.e., increasing) the objective function for constraint violations. Although both methods are effective, there is substantial discussion on the limitations of both methods. Nour-Omid [Ref. 3] described the positive and negative aspects of both methods. The Lagrange method has been shown to be the more accurate method. However, its usage requires the introduction of additional unknowns thus increasing the

system's degrees-of-freedom and computational time. The penalty method does not require additional computational time, but it has been shown to result in less accurate solutions in satisfying the contact boundary conditions. Since the contact boundary conditions are exactly satisfied only when the penalty term goes to infinity, the correct choice of the penalty parameter is the key to an acceptable solution. Guerra [Ref. 4] supported these claims.

Because of the limitations of the Lagrange and penalty methods, Bishoff [Ref. 5] advocated the use of the augmented Lagrange multiplier method to solve finite element contact problems. This method is favorable since it avoids the limitations of both methods discussed above. The augmented Lagrange multiplier method is similar to the penalty method in that the objective function is penalized for constraint violations. However, an additional multiplier term is added so the optimum can be achieved by a combination of both terms. As stated by Vanderplaats [Ref. 6: p. 141], the advantage of this method is that the penalty term is not required to grow to infinity to achieve exact constraint satisfaction.

The augmented Lagrange multiplier method can be used in numerical programming techniques to find the optimum of any functional. Pierre and Lowe [Ref. 7] provide a detailed analysis of the programming techniques necessary in applying this method. Additionally, Vanderplaats [Ref. 6: pp. 140-147] provided an excellent discussion on the practical usage of this method in numerical techniques. Rothert et al. [Ref. 8] used a numerical programming code based on this method to solve a nonlinear contact problem. In this study, an existing numerical optimization routine utilizing the augmented Lagrange multiplier method will be used as an integral part of two solution methods developed to solve the contact problem. These methods will use different techniques to obtain the same functional. The augmented Lagrange multiplier method will then be used in a similar fashion to solve each problem. In each case, the optimization routine will be used to determine a set of design variables that describes the contact state.

Following the development and verification of the numerical procedures, this study will investigate the response of composite sandwich materials to low velocity impact. One of the common failure mode of low velocity impact is delamination. Joshi and Sun [Ref. 9] studied the impact response of a three layer cross-ply graphite epoxy laminate. A correlation was obtained between delamination cracks initiated experimentally and maximum shear stress points determined numerically. Sun and Rechak [Ref. 10] followed up these findings and found that the introduction of adhesive layers between laminae reduced the shear stress distribution thus reducing delamination. Choi, Wang,

and Chang [Ref. 11] studied the effects of laminae orientation, ply thickness, and stacking sequence on impact damage of graphite epoxy composites. It was determined that stacking sequence affects impact damage more than laminae thickness variations. Much of the previous work has focused on the behavior of the graphite epoxy laminate. However, there is currently interest in the development of turbine blades constructed of sandwich composites. It is therefore beneficial to investigate the response of composite sandwich materials to low velocity impact.

II. FORMULATION OF THE CONTACT PROBLEM

A. PRINCIPLE OF MINIMUM TOTAL POTENTIAL ENERGY

As discussed in the introduction, the limited utility of the analytical solutions necessitated the development of solution techniques capable of handling the nonlinear behavior of the contact problem with complicated geometry and complex boundary conditions. This study intends to develop two numerical procedures to solve the contact problem. In short, the procedures will use different methods to obtain a functional, the system's total potential energy, and then use similar methods to obtain the equilibrium condition. Determination of the equilibrium position is made by application of the principle of minimum potential energy. With equilibrium established, contact stresses can be quantified. In order to understand the details of this approach, the principle of virtual work and the principle of minimum potential energy must be discussed.

Given a body in equilibrium, it is desired to describe the response of that body to infinitesimal displacements resulting from a system of forces. If each particle in the body is described by some generalized coordinates, then the work resulting from these infinitesimal displacements is simply the product of the generalized forces acting on each particle and the particle's displacement. However, if the particle is in equilibrium, the work must be zero since the summation of forces in the x, y, and z directions is zero. The infinitesimal displacements and work in this example are referred to as virtual in nature. The fact that this work vanishes is referred to as the principle of virtual work.

The virtual work discussed thus far can be subcategorized as virtual strain energy and virtual work done by external forces. From the definition of strain energy, virtual strain energy, δU , that results from virtual displacements can be calculated. Since this energy is viewed as energy against the bonds between elements, δU is a negative quantity. The work done by external forces is designated δW and is simply the summation of the product of the external forces and the displacements of the generalized coordinates.

Since the principle of virtual work states that the work done as a result of virtual displacements is zero,

$$\delta W - \delta U = 0$$

Alternately, this can be expressed as,

$$\Pi = \delta(U - W) = 0$$

where Π represents the system's total potential.

The above equation illustrates the condition of minimum total potential of a system. This is the foundation of the principle of minimum potential energy. [Ref. 12: pp. 330-331] This principle states that in a condition of stable equilibrium, the system's total potential is stationary. Hence, determination of a system's total potential energy and the minimization of that quantity will enable the calculation of the equilibrium position. This is the basis for the numerical techniques developed in this study.

B. CONTACT PROBLEM DESCRIPTION

The objective of the solution techniques to be developed is to obtain a means of calculating the total potential energy and minimize it to determine the equilibrium condition. To accomplish this, two different models will be created to first solve a simple isotropic case, the solution of which is known. In this manner, our models can be validated for use in more complicated arrangements.

Consider contact between a cylinder and an infinite plane as shown in Figure 1. A cross section of the contact zone is shown in Figure 2. Let the width of the contact zone equal a distance of $2a$. An analytical solution of this problem is available as a result of the work done by Hertz. In developing the solution methods, only a very limited region adjacent to the contact zone will be examined. The reason for this is that the contact phenomenon is a very local one. Figure 3 represents the analytical solution of the normal stresses resulting from this contact problem. [Ref. 13] As shown, the stresses in the foundation diminish very rapidly. The diagram shows that σ_x becomes negligible at depths less than one half-contact zone (a) and σ_y diminishes significantly in less than 3 half zones. Because of this, it is reasonable to assume that displacements beyond a very limited region are negligible in the strain energy calculation of the contact problem.

A number of simplifying assumptions will be made for this study:

1. As discussed above, displacements beyond a limited region are negligible in strain energy calculations.
2. The foundation is an elastic isotropic material. The cylinder (roller) is rigid.

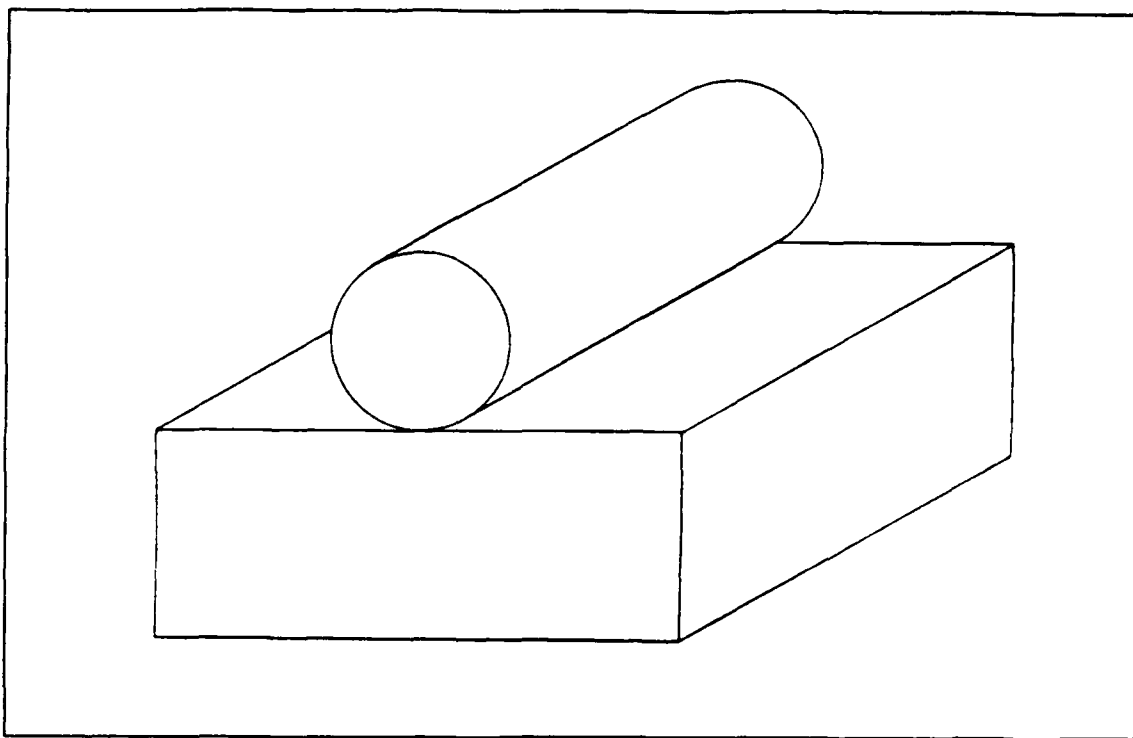


Figure 1. Roller-foundation assembly

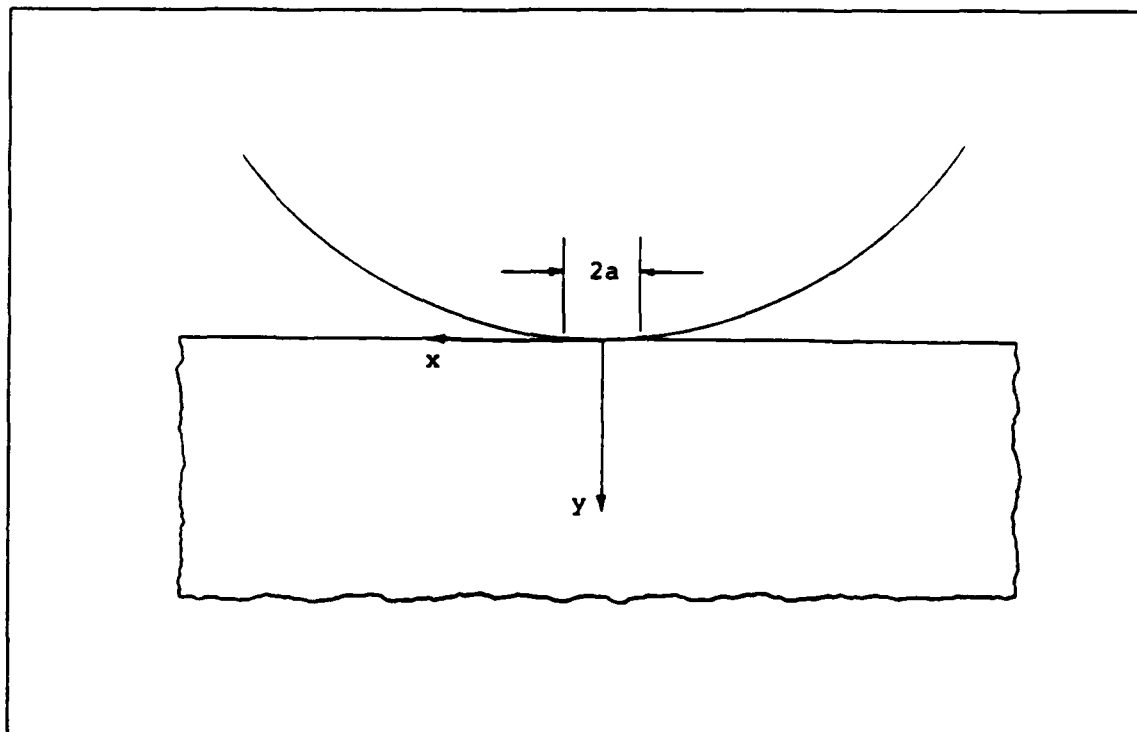


Figure 2. Contact zone cross section

3. Deformations normal to the cross-section are negligible, hence a condition of plane strain exists.
4. The roller is subjected to a vertical distributed load.
5. The roller-foundation contact is frictionless.

An important restriction on the minimization problem will be that one body will be prohibited from penetrating into the other body. This may seem like an obvious restriction, however a method of mathematically stating this restriction must be discussed. Figure 4 shows the deformed and undeformed contact zone. Let δ represent the deflection of the roller due to an external force and $v(x,y)$ represent the vertical deflection of the foundation at any point (x,y) . At the point of Contact A, the condition of no interference can be expressed as,

$$v(0,0) \geq \delta$$

At point B, this condition can be stated as,

$$v(r \sin \theta, 0) \geq \delta - r(1 - \cos \theta)$$

The latter condition can be specified at as many points as necessary to define this restriction.

C. NUMERICAL OPTIMIZATION

1. Optimization Fundamentals

Before developing the models to be used in this study, one final area must be discussed. Once the total potential energy has been calculated, a method of minimizing it to find the equilibrium position must be employed. A study of the numerical optimization technique to be used is required.

The technique being used in this study relies heavily on the methods of design optimization. Design optimization is the utilization of mathematical techniques to minimize or maximize a particular value to obtain an optimum solution. The method is ideally suited for design. A given design task may have an infinite number of solutions. However, finding the best solution is a matter of the designer's experience and intuition. In the absence of significant experience in a particular field, finding this solution may reduce to examining a range of possible solutions by trial and error. Optimization routines can be utilized to find this solution mathematically.

Optimization problems can be constrained or unconstrained. For example, it may be desired to determine the minimum of the parabola, $F(x) = (x - 5)^2 + 2$. As seen

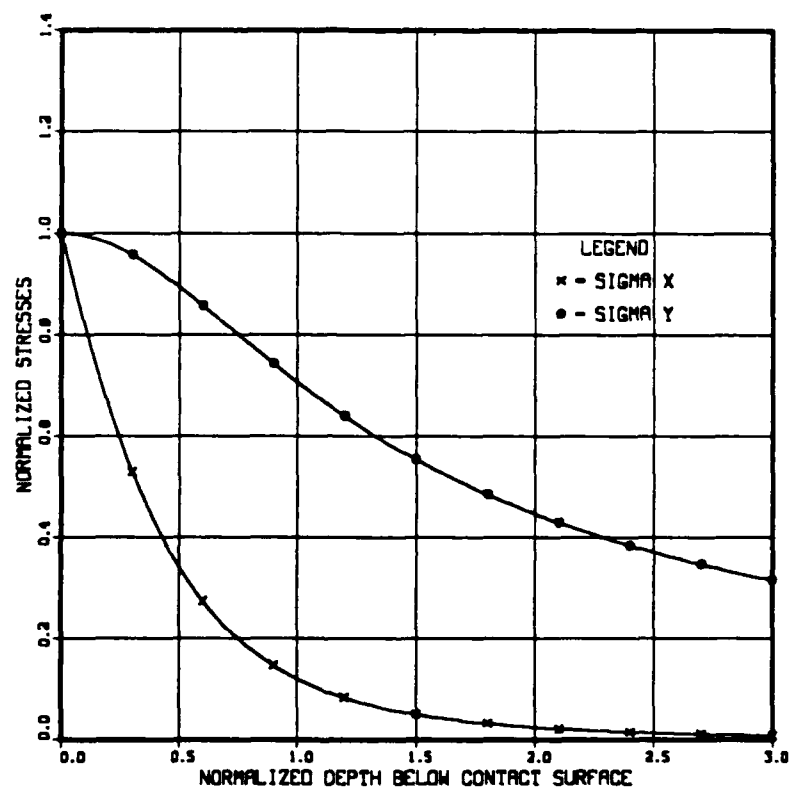


Figure 3. Analytical solutions for σ_y and σ_x .

in Figure 5, the minimum is clearly identified at point A. This is an example of an unconstrained problem. A constrained counterpart of this problem is:

Minimize: $F(x)$

Subject to: $F(x) \geq .5x + 4$

As seen in Figure 6, the minimum of the constrained problem is at point B. This is a simple illustration of constrained minimization. The contact problem is a constrained minimization problem.

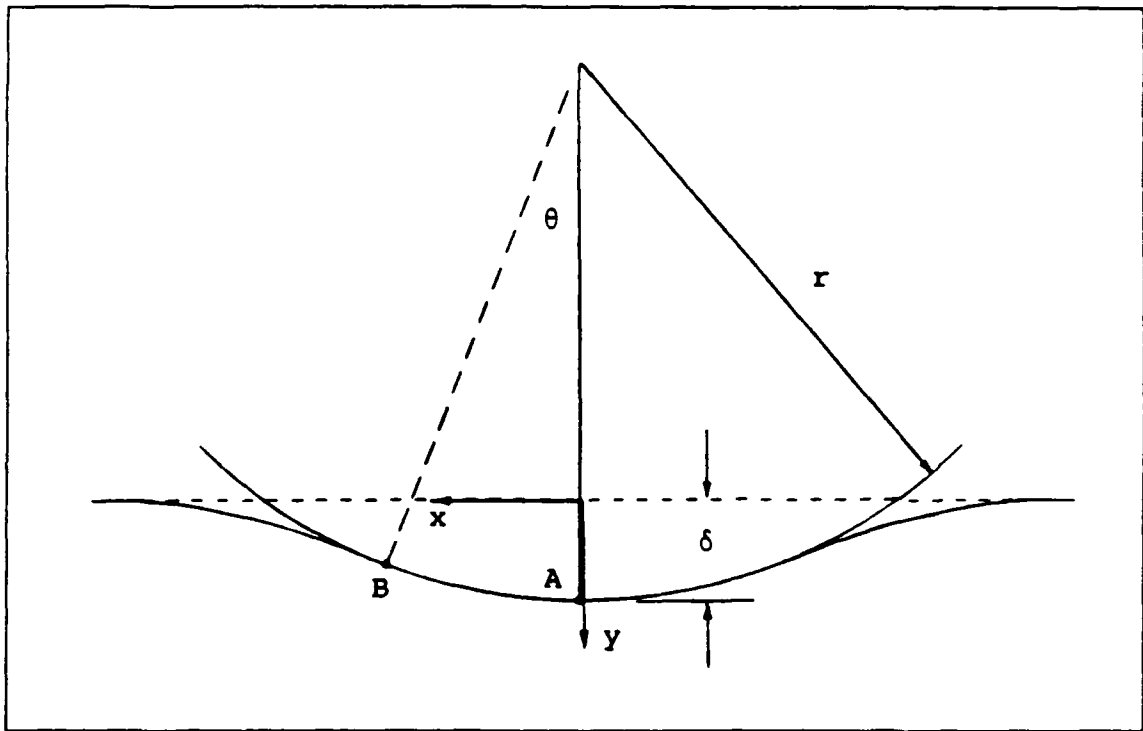


Figure 4. Deformed contact zone

The value to be minimized or maximized is referred to as the objective function. The parameters to be determined are referred to as design variables. The optimization process is an iterative one. The objective function is evaluated. The design variables are varied thus obtaining a new objective function. If the difference is within a certain tolerance or meets a certain convergence criteria, the optimum has been obtained. If it is out of tolerance, the cycle repeats.

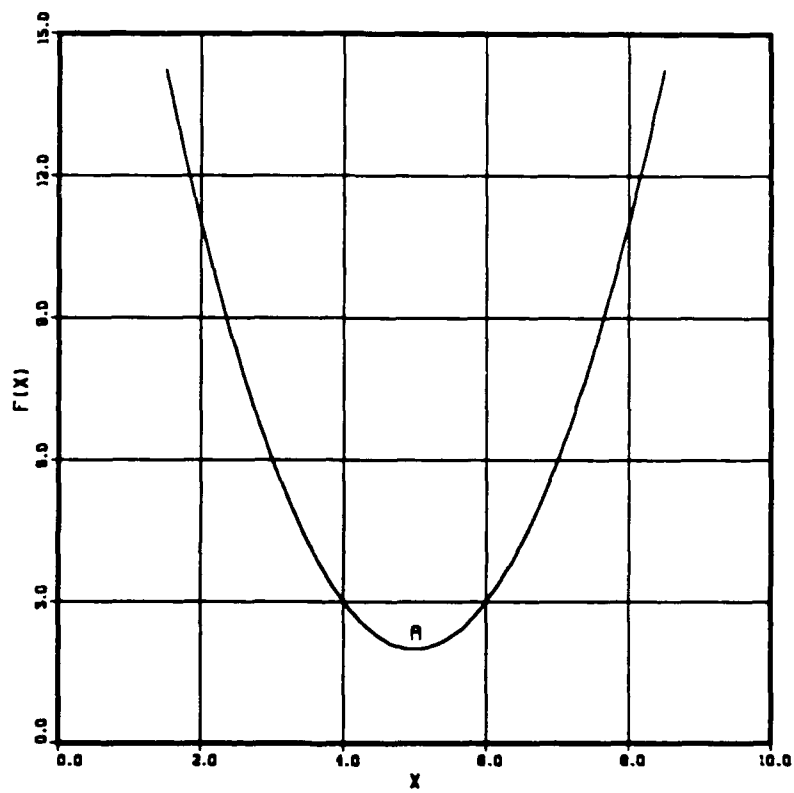


Figure 5. Unconstrained minimization

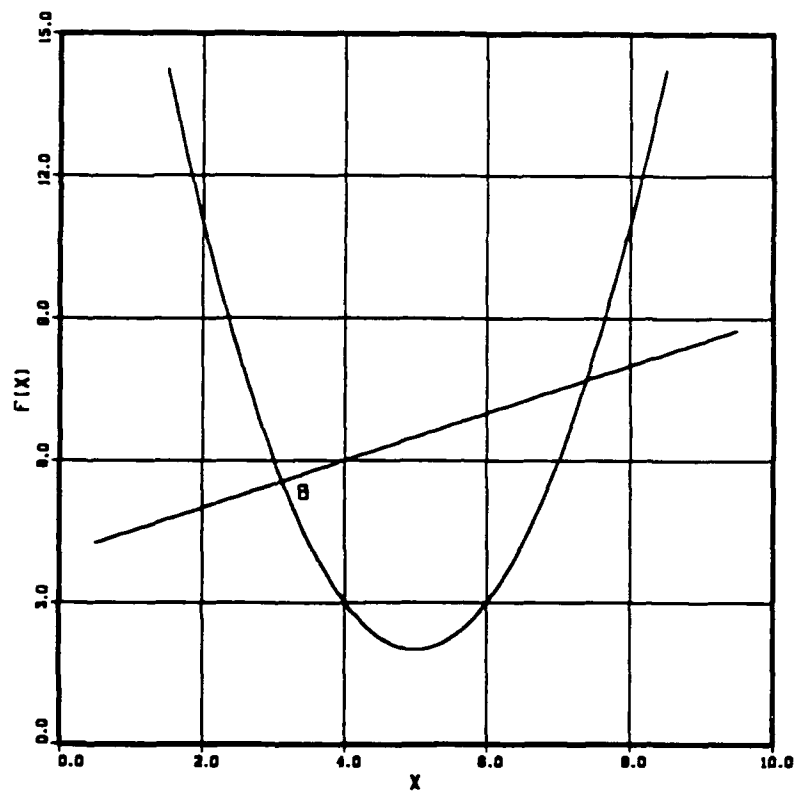


Figure 6. Constrained minimization

2. Augmented Lagrange Multiplier Method

The contact problem belongs in the class of constrained problems. There are several techniques of solving constrained problems. The technique used in this study belongs to a class of solution techniques known as sequential unconstrained minimization techniques (SUMT). This class of techniques is designed for the general nonlinear problem. The fundamental concept behind this approach is that a constrained problem is transformed into an unconstrained problem and the objective function is minimized using an unconstrained minimization technique. This transformation is accomplished by assessing a penalty to the objective function for constraint violations. For example, if the design variables are varied in such a way as to enter the region where a constraint is violated (i.e., the infeasible region), the objective function would be assessed a penalty (i.e., increased). Thus, in order to minimize the objective function, the design variables remain within the region where no constraints are violated (i.e., the feasible region). [Ref. 6: pp. 121-123]

There are a number of methods within this class of techniques. They essentially differ in the way in which penalties are assessed. The technique used in this study is the augmented Lagrange multiplier (ALM) method.

Given the constrained inequality optimization problem:

$$\begin{aligned} \text{Minimize: } & F(X) \\ \text{Subject to: } & g_i(X) \leq 0, i = 1, 2, \dots, n \end{aligned}$$

The Augmented Lagrangian is defined as,

$$A(X, \lambda, p) = F(X) + \sum_{i=1}^m \{ \lambda_i [g_i(X) + s_i^2] + p [g_i(X) + s_i^2]^2 \}$$

where,

$X \equiv$ vector containing the design variables

$\lambda_i \equiv$ Lagrange multipliers

$p \equiv$ penalty parameter

$s_i \equiv$ slack variables which convert inequality constraints to equality constraints

The first two terms of $A(X, \lambda, p)$ represent the Lagrangian. From the method of Lagrange multipliers, it is known that minimization of the Lagrangian represents optimality. Like simple problems where λ is simply an additional unknown to obtain, in the ALM method λ is unknown. Hence, a mathematical routine based on constraint values is used to select and modify λ for successive iterations. [Ref. 6: pp. 140-147] Initial selection of this term can have a significant impact of the problem's convergence.

As discussed above, a penalty is assessed to the objective function for constraint violations. This feature is apparent by examining the last term. A constraint violation results in a positive value for $g(X)$ thus resulting in an increase in A . The value of p is a scaling term which is sequentially increased throughout optimization. This ensures that there is a balance between convergence and numerical conditioning. If p remains small, convergence may occur with major constraint violations. If p remains large, constraints will be satisfied at the expense of an ill-conditioned problem [Ref. 7: p. 169]. As with the Lagrange term, selection of this term has a significant impact on the outcome of the problem.

3. Optimizer and One-Dimensional Search

Thus far, a procedure has been defined which has transformed a constrained minimization problem into an unconstrained one. This level of the optimization process is referred to as the optimization strategy. The formulation of the modified objective function via the augmented Lagrange multiplier method represents a key portion of the optimization process. However, there are additional parts of this process that require comment.

With the modified objective function and a procedure for assessing penalties in place, a procedure for minimizing the objective function must be defined. This portion of the process is carried out by the 'optimizer.' The optimizer's function is to systematically alter the design variables in a manner that reduces the objective function rapidly. If X represents a vector containing the design variables, the following process is used by the optimizer to alter X

$$X_i = X_{(i-1)} + k_i S_i$$

where,

$i \equiv$ current iteration number

$S \equiv$ search vector

$k \equiv$ scalar representing distance traveled in direction S

In general, two processes must be accomplished to find the optimum. First, the search direction S must be determined by a systematic process. An example of this phase is the steepest descent method where the direction of steepest gradient is chosen. Second, the scalar k must be determined such that the objective function is minimized as much as possible in the search direction of the current iteration. The latter phase is referred to as one-dimensional search. [Ref. 6: pp. 10-12]

The optimizer used in this study is the variable metric method. Due to the complexity of this method, a discussion of their formulation is omitted. A detailed account is available in Vanderplaats [Ref. 6: pp. 92-93]. The one-dimensional search routine used in this study is the golden section method with polynomial interpolation. The one-dimensional search portion of the process merely represents a systematic and efficient method of finding the minimum in the chosen search direction. A detailed account of this approach is again available in Vanderplaats [Ref. 6: pp. 26-49].

4. Convergence

The final point to be discussed relevant to optimization fundamentals is that of convergence. Convergence criteria are utilized to identify the optimum solution and terminate calculations. There are a number of convergence criteria that can be utilized. The most obvious is absolute convergence where the objective functions from two successive iterations are compared. If the difference between the values is within some prescribed limit, optimization is terminated. A second method signifying optimality for unconstrained problems is calculation of the gradient with respect to the design variable vector X . If this value is approximately zero, optimality has been achieved. This method is called the Kuhn-Tucker conditions for unconstrained minimization. Kuhn-Tucker conditions are more involved for constrained problems. [Ref. 6: pp. 100-101]

The Automated Design Synthesis (ADS) System used in this study uses both these termination criteria as well as relative convergence. Relative convergence is similar to absolute convergence except normalized versions of the difference between successive iterations is calculated. Again, if a specified tolerance is achieved, optimization is terminated.

III. APPROXIMATE SOLUTION TECHNIQUES

A. RAYLEIGH-RITZ APPROACH

1. Background

The Rayleigh-Ritz method is a method of utilizing the theory of minimum potential energy to solve a given problem. The fundamental concept behind this method is that a trial function that represents the deformation field is chosen in terms of unknown constants. Second, the system's total potential energy is calculated in terms of the trial function. Since the total potential is a minimum at equilibrium, minimization enables determination of the unknown constants. The total potential is minimized by differentiating with respect to the unknown constants and equating to zero. The result is 'n' equations and 'n' unknowns, the trial function constants. [Ref. 12: pp. 335-336]

The only requirement of the Rayleigh-Ritz method is that the trial function is kinematically admissible. A kinematically admissible solution is one that satisfies the geometric boundary conditions of the system (i.e., deflection and slope). Other requirements need not be satisfied. As an example, consider a simply supported beam of length L with the origin at the left end of the beam. A kinematically admissible solution to describe the beam's one dimensional deformation from vertical loading in the y direction is,

$$y(x) = a_n \sin\left(\frac{\pi x}{L}\right)$$

where a_n represents the coefficient to be determined.

Deflection boundary conditions at $x = 0$ and $x = L$ have been satisfied. Obviously, an increased number of terms in the trial function will yield a far more accurate solution. A Fourier sine series would be a reasonable selection in this case.

Although the Rayleigh-Ritz method does not stipulate numerous requirements on the trial function, sensible choices of trial functions will increase solution accuracy significantly. For example, consider the same simply supported beam with the origin now at the center. A kinematically admissible function is,

$$y(x) = a_n \sin\left(\frac{2\pi x}{L}\right).$$

Naturally however, due to the placement of the origin in this problem, an even function is a much for sensible selection for a trial function. A more appropriate selection would be,

$$y(x) = a_n \cos\left(\frac{\pi x}{L}\right).$$

The latter point concerning sensible selection of the trial function will be discussed in detail throughout this study.

2. Application of the Rayleigh-Ritz Method to the Contact Problem.

A brief overview of the method to be developed is in order. Application of the Rayleigh-Ritz method necessitates the selection of the appropriate trial function in terms of unknown coefficients. A discussion of the physical nature of this problem as well as the desired features of the trial solution is required.

The theory of elasticity relationships will be applied using the trial function to obtain the system's strain energy in terms of unknown coefficients. The system's total potential energy will then be minimized utilizing the optimization techniques discussed in Chapter II. The design variables are the unknown trial function coefficients. With the coefficients determined, the displacement is known for all points enabling the stress to be determined throughout the body. Figure 7 is a flow chart of the procedure to be utilized. The post-processing procedure shown is simply the calculation of the stresses using the now determined coefficients.

3. Trial Function Selection

In order to choose an appropriate trial function, it is necessary to have an understanding of the physical phenomena to be modeled. Consider the roller-foundation system shown in Figure 1. Two trial functions are needed to model horizontal and vertical deformation. There are a number of important characteristics that should be inherent within the trial functions. These are outlined below:

1. As seen in Figure 3, σ_x and σ_y are equal and compressive at the point of contact. Additionally, σ_x decays more rapidly than σ_y as distance from the contact point increases.
2. Taking the origin at the point of contact as shown in Figure 2, the u-deformation takes the form of an odd function.
3. The v-deformation takes the form of an even function (i.e. symmetric about the origin and greatest at the origin).
4. To satisfy the Rayleigh-Ritz method requirements, the boundary conditions must be satisfied. In this case, this requires u and v deformation to be zero at the far boundaries.

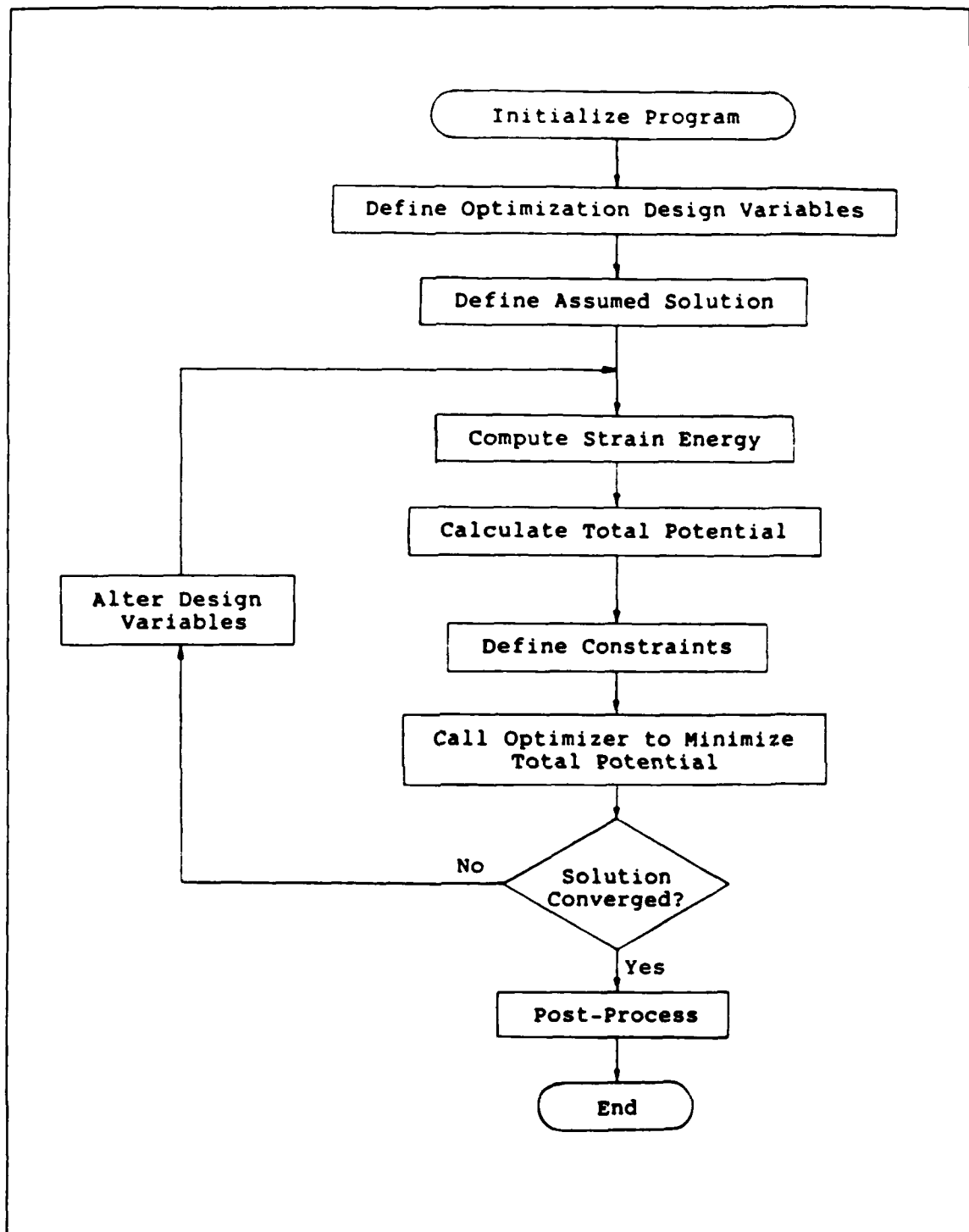


Figure 7. Rayleigh-Ritz method applied to contact problem

5. The characteristics outlined in item 4 satisfy the requirements of this method. However, since this study will be a stress analysis, it is also desired that the stresses also reflect the physical phenomena. Since σ_x and σ_y are functions of x , and ϵ_x and ϵ_y should also exhibit certain characteristics. Referring to Figure 8 for dimensions and the coordinate system, it is desired that ϵ_x and ϵ_y equal zero at $x = L/2$ and $y = H$. This will ensure that stresses are zero at the boundaries. To satisfy the requirements of item 1 above, ϵ_x and ϵ_y should be equal and negative at the point of contact and decrease in magnitude as the distance from the point of contact increases.

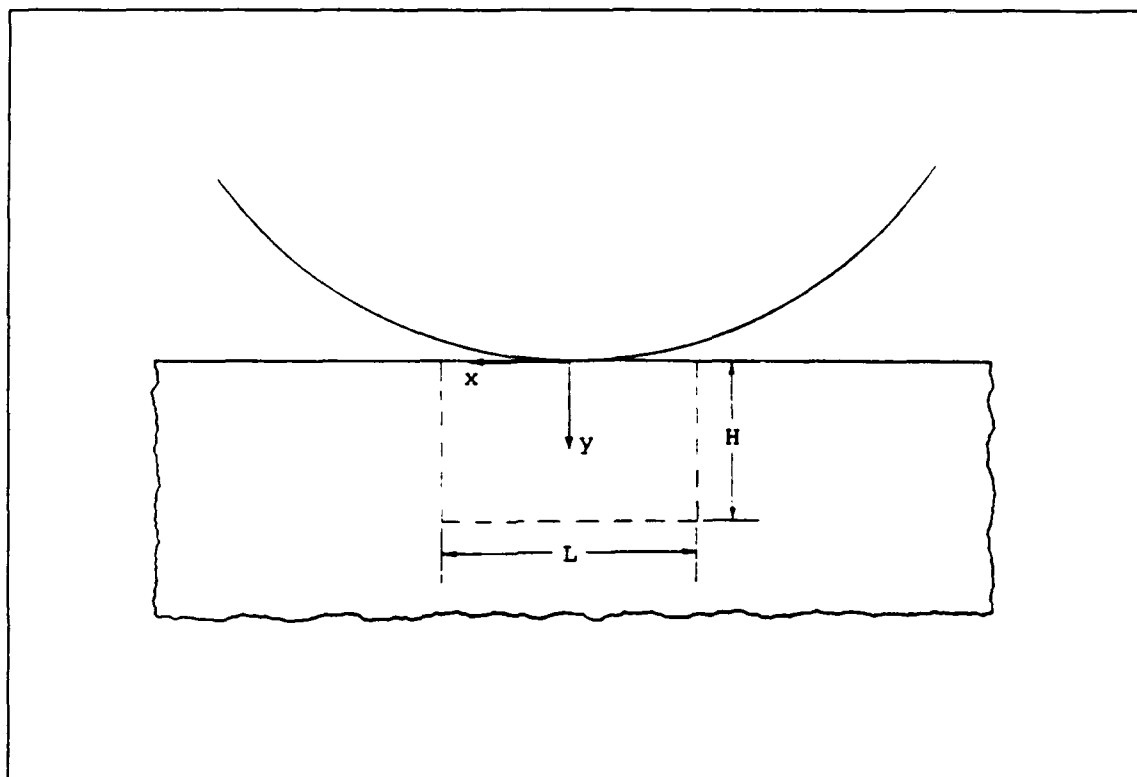


Figure 8. Contact zone

With the above guidelines in mind, the trial function can be selected. The trial functions chosen for this study are composed of a series of terms of the general form:

$$u(x,y) = a_n(H-y)^a \left(\frac{L}{2} - x \right)^b \quad (3.1)$$

$$v(x,y) = b_n(H-y)^c \left(\frac{L}{2} - x \right)^d \quad (3.2)$$

These expressions were carefully chosen and represent a compromise due to the difficulties of satisfying all boundary conditions with the physical phenomena of this problem.

From the above expressions, it is immediately obvious that the geometric boundary conditions at $x = L/2$ and $y = H$ have been satisfied. This satisfies the requirements of the Rayleigh-Ritz method. In addition, there are a number of important characteristics that illustrate the advantage of this selection:

1. ϵ_x and ϵ_y are negative thus simulating a compressive environment in the vicinity of the point of contact. The importance of this is obvious. If normal strains were not negative, the resulting requirement would be for the coefficient to be less than zero to simulate compression. It is obvious that this would result in deformations opposite to that which was desired by the choice of the trial function.
2. This selection for deformation fields has the important characteristic of decreasing deformation as we move away from the point of contact. Also note that deformation is maximum at the point of contact.
3. The exponents a, b, c, and d can be varied to simulate subsurface stress fields. For example, if the analytical solution indicates a large y gradient for σ_x at $x=0$, the objective would be to increase the rate at which ϵ_x decreases as the distance from the point of contact increases. This would be easily simulated by raising the value of a. If this change had a detrimental effect on the behavior of σ_y , the exponents of the vertical deformation could be varied to restore the solution.

It is important to note that this selection is not without compromise. The most significant limitation of the trial functions is with regard to the horizontal deformation u . Physically, it is expected the $u(x,y)$ behave as an odd function as discussed above. However, in this selection of trial function, a positive value of $u(x,y)$ exists at the origin. This is contrary to the physical behavior of the problem and will lead to some error. However, considering that the magnitude of this deformation in the elastic range is small, this error is believed to be limited. Another consequence of this compromise is the existence of non-zero shear strain at $x = 0$.

Another less severe limitation is a restriction on the order of the exponents in order to maintain zero stress at the boundaries. Since σ_x and σ_y are combinations of ϵ_x and ϵ_y , both normal strains must be zero at the boundaries to ensure that stresses are zero at these locations. Since the normal strains are first derivatives, this requires that b and c are at least equal to 2.

It is worthwhile to note that most of the considerations discussed above far exceed the requirements stipulated by the Rayleigh-Ritz method. The objective has been to utilize trial functions that closely match the physical nature of the problem in an effort to maximize accuracy.

The specific trial functions used in this study are listed below. The horizontal deformation was assumed to be;

$$u(x,y) = \sum_{n=1}^m a_n (H-y)^{(4+n)} \left(\frac{L}{2} - x \right)^2 \quad (3.3)$$

where H and L represent the height and length of the bearing foundation, respectively. Summation was done for n equal 1 and 4. The vertical deformation was assumed to be;

$$v(x,y) = \sum_{n=1}^m b_n (H-y)^2 \left(\frac{L}{2} - x \right)^{(1+n)}. \quad (3.4)$$

As discussed previously, manipulation of the exponents enables the trial function results to be matched with the analytical solution. As will be illustrated in the results, the exponents chosen in the above functions achieve this goal sufficiently.

With the deformations chosen, the stresses and strains can be calculated for use in the calculation of the foundation strain energy. These values are shown below:

$$\epsilon_x = \sum_{n=1}^m -2a_n (H-y)^{(4+n)} \left(\frac{L}{2} - x \right) \quad (3.5)$$

$$\epsilon_y = \sum_{n=1}^m -2b_n (H-y) \left(\frac{L}{2} - x \right)^{(1+n)} \quad (3.6)$$

$$\sigma_x = \frac{E}{(1+\nu)(1-2\nu)} [(1-\nu)\epsilon_x + \nu\epsilon_y] \quad (3.7a)$$

$$\sigma_y = \frac{E}{(1+\nu)(1-2\nu)} [(1-\nu)\epsilon_y + \nu\epsilon_x] \quad (3.7b)$$

where E and ν are Young's modulus and Poisson's ratio, respectively. For the shear stress and strain,

$$\frac{\partial u}{\partial y} = \sum_{n=1}^m -(4+n)a_n (H-y)^{(3+n)} \left(\frac{L}{2} - x \right)^2 \quad (3.8)$$

$$\frac{\partial v}{\partial x} = \sum_{n=1}^m -(1+n)b_n (H-y)^2 \left(\frac{L}{2} - x \right)^n \quad (3.9)$$

$$\gamma_{xy} = \frac{\partial u}{\partial y} + \frac{\partial v}{\partial x} \quad (3.10)$$

$$\tau_{xy} = G\gamma_{xy} \quad (3.11)$$

where G is the shear modulus.

Using the above quantities, the strain energy U can be calculated. From the definition of strain energy applied to a two dimension deformation field,

$$U = \int_{-\frac{L}{2}}^{\frac{L}{2}} \int_0^H \frac{1}{2} (\sigma_x \epsilon_x + \sigma_y \epsilon_y + \tau_{xy} \gamma_{xy}) dy dx \quad (3.12)$$

Because of symmetry about the origin, strain energy can be calculated for half of the domain and doubled. With strain energy calculated, the total potential for the system can be found from,

$$\Pi = U - F\delta \quad (3.13)$$

where,

$F \equiv$ external force per unit length applied to the roller

$\delta \equiv$ vertical distance traveled by the roller.

The quantity $F\delta$ represents the work done by the roller on the bearing foundation.

B. FINITE ELEMENT APPROACH

1. Total Potential Derivation

The finite element method can be employed to solve the contact problem. A finite element mesh can be constructed to approximate the behavior of an elastic foundation subjected to line contact loading from an rigid roller. The resultant interaction between the foundation and roller enables the calculation of the foundation's strain energy and the subsequent calculation of the total potential energy. By again utilizing the optimization techniques discussed in Chapter II, the equilibrium position can be determined. Thus the contact stresses can be calculated throughout the body.

The objective is to derive a means of calculating the total potential of the system by application of the finite element technique. Total potential energy is defined as,

$$\Pi = U - F\delta \quad (3.14)$$

where,

$U \equiv$ internal strain energy

$F \equiv$ external force per unit length applied to the roller

$\delta \equiv$ vertical distance traveled by the roller.

The strain energy of the system can be found from,

$$U = \int_{\Omega} \frac{1}{2} (\sigma_x \epsilon_x + \sigma_y \epsilon_y + \tau_{xy} \gamma_{xy}) d\Omega \quad (3.15)$$

where Ω represents the problem domain. This can be expressed in matrix form as,

$$U = \int_{\Omega} \frac{1}{2} \{\epsilon\}^T \{\sigma\} d\Omega \quad (3.16)$$

where,

$$\{\epsilon\}^T = \{\epsilon_x \quad \epsilon_y \quad \gamma_{xy}\}$$

$$\{\sigma\}^T = \{\sigma_x \quad \sigma_y \quad \tau_{xy}\}$$

On the element level,

$$U = \int_{\Omega^i} \frac{1}{2} \{\epsilon\}^T \{\sigma\} d\Omega \quad (3.17)$$

where i represents analysis of the i^{th} element.

The stress matrix can be expressed as,

$$\{\sigma\} = [D]\{\epsilon\} \quad (3.18)$$

where $[D]$ represents the material property matrix.

For a condition of plane strain, the stiffness matrix can be expressed as,

$$[D] = \frac{E}{(1+v)(1-2v)} \begin{bmatrix} 1-v & v & 0 \\ v & 1-v & 0 \\ 0 & 0 & \frac{1-2v}{2} \end{bmatrix} \quad (3.19a)$$

For a plane stress condition,

$$[D] = \frac{E}{(1-v^2)} \begin{bmatrix} 1 & v & 0 \\ v & 1 & 0 \\ 0 & 0 & \frac{1-v}{2} \end{bmatrix} \quad (3.19b)$$

The development of this technique will use linear triangular elements. The method, however, can be applied to any type element. For linear triangular element, the deformations take the following form:

$$u = H_1 u_1 + H_2 u_2 + H_3 u_3 \quad (3.20)$$

$$v = H_1 v_1 + H_2 v_2 + H_3 v_3 \quad (3.21)$$

where the shape functions H_i are defined as:

$$H_1 = [(x_2 y_3 - x_3 y_2) + (y_2 - y_3)x + (x_3 - x_2)y] \frac{1}{2A} \quad (3.22)$$

$$H_2 = [(x_3 y_1 - x_1 y_3) + (y_3 - y_1)x + (x_1 - x_3)y] \frac{1}{2A} \quad (3.23)$$

$$H_3 = [(x_1 y_2 - x_2 y_1) + (y_1 - y_2)x + (x_2 - x_1)y] \frac{1}{2A} \quad (3.24)$$

where,

x_i, y_i = coordinates for node i

A = element area [Ref. 14].

The strain matrix can be expressed as,

$$\{\epsilon\} = \begin{bmatrix} \frac{\partial}{\partial x} & 0 \\ 0 & \frac{\partial}{\partial y} \\ \frac{\partial}{\partial y} & \frac{\partial}{\partial x} \end{bmatrix} \begin{Bmatrix} u \\ v \end{Bmatrix} \quad (3.25)$$

Substituting equations (3.20) and (3.21) into equation (3.25) yields,

$$\{\epsilon\} = \begin{bmatrix} \frac{\partial H_1}{\partial x} & 0 & \frac{\partial H_2}{\partial x} & 0 & \frac{\partial H_3}{\partial x} & 0 \\ 0 & \frac{\partial H_1}{\partial y} & 0 & \frac{\partial H_2}{\partial y} & 0 & \frac{\partial H_3}{\partial y} \\ \frac{\partial H_1}{\partial y} & \frac{\partial H_1}{\partial x} & \frac{\partial H_2}{\partial y} & \frac{\partial H_2}{\partial x} & \frac{\partial H_3}{\partial y} & \frac{\partial H_3}{\partial x} \end{bmatrix} \begin{bmatrix} u_1 \\ v_1 \\ u_2 \\ v_2 \\ u_3 \\ v_3 \end{bmatrix} \quad (3.26)$$

In abbreviated notation, equation (3.26) is expressed as,

$$\{\epsilon\} = [B]\{d\} \quad (3.27)$$

For the linear triangular element, $[B]$ reduces to,

$$[B] = \frac{1}{2A} \begin{bmatrix} y_2 - y_3 & 0 & y_3 - y_1 & 0 & y_1 - y_2 & 0 \\ 0 & x_3 - x_2 & 0 & x_1 - x_3 & 0 & x_2 - x_1 \\ x_3 - x_2 & y_2 - y_3 & x_1 - x_3 & y_3 - y_1 & x_2 - x_1 & y_1 - y_2 \end{bmatrix} \quad (3.28)$$

Returning to the element strain energy calculation, equation (3.17),

$$U = \int_{\Omega'} \frac{1}{2} \{\epsilon\}^T \{\sigma\} d\Omega$$

and substituting (3.18) into (3.17),

$$U = \int_{\Omega'} \frac{1}{2} \{\epsilon\}^T [D] \{\epsilon\} dV. \quad (3.29)$$

Substituting equation (3.27) yields,

$$\begin{aligned}
 U &= \int_{\Omega} \frac{1}{2} ([B]\{d\})^T [D][B]\{d\} dV \\
 U &= \frac{1}{2} \{d\}^T [B]^T [D][B]\{d\} \int_{\Omega} dV \\
 U &= \frac{1}{2} \{d\}^T [B]^T [D][B] A t \{d\}
 \end{aligned} \tag{3.30}$$

where t = unit depth. Defining the element stiffness matrix $[K]$,

$$[K] = [B]^T [D][B] A t \tag{3.31}$$

then the strain energy per element equals,

$$U = \frac{1}{2} \{d\}^T [K]\{d\} \tag{3.32}$$

The element stiffness matrix can be expanded into the global stiffness matrix. With strain energy now determined, total potential can be determined from equation (3.14).

2. Optimization and Static Condensation

As with the previously developed model, the augmented Lagrange multiplier method will be utilized to determine the equilibrium condition via the theorem of minimum potential. The objective function is again the total potential. In this case, however, the design variables are the nodal deformations, u_i and v_i , for non-fixed nodes. Constraint equations are developed in a similar manner as discussed in Chapter II to ensure that one body does not violate space occupied by the other.

Since the nodal deformations are represented as the optimization design variables, the number of design variables will equal twice the number of non-fixed nodes. For a simple mesh, a direct application of this procedure will likely yield accurate results. However, it is known that the accuracy of the optimization routine declines as the number of design variables increases. Hence, for complicated finite element meshes, solution accuracy will be adversely affected by the large number of design variables. Therefore a procedure must be adopted to eliminate the need for assigning design vari-

ables to nodes where information is not necessary for evaluating a solution. This procedure is known as static condensation.

Static condensation has been utilized by References 2 and 3 in an effort to reduce computer computational time. The idea behind static condensation is the reorganization of the global stiffness matrix. A finite element problem can be expressed as,

$$[K_g]\{u\} = \{F\} \quad (3.33)$$

where,

$[K_i]$ = the stiffness matrix

$\{u\}$ = the deformation vector

$\{F\}$ = the force vector

It is desired to reorganize this system of equations into the following:

$$\begin{bmatrix} K_{11} & K_{12} \\ K_{21} & K_{22} \end{bmatrix} \begin{Bmatrix} u_1 \\ u_2 \end{Bmatrix} = \begin{Bmatrix} F \\ 0 \end{Bmatrix} \quad (3.34)$$

The vector u_1 contains the essential nodes while vector u_2 contains non-essential nodes. Essential nodes are those where boundary conditions are applied and nodes that are assigned optimization design variables. By matrix manipulation,

$$\{u_2\} = -[K_{22}]^{-1}[K_{21}]\{u_1\}. \quad (3.35)$$

Therefore, the displacement vector can be expressed as,

$$\begin{Bmatrix} u_1 \\ u_2 \end{Bmatrix} = \begin{Bmatrix} \{u_1\} \\ -[K_{22}]^{-1}[K_{21}]\{u_1\} \end{Bmatrix} = \begin{bmatrix} [I] \\ -[K_{22}]^{-1}[K_{21}] \end{bmatrix} \{u_1\} \quad (3.36)$$

where I represents the identity matrix.

Substituting this equation into the global counterpart of equation (3.32),

$$U = \frac{1}{2} \{u_1\}^T \begin{bmatrix} [I] \\ -[K_{22}]^{-1}[K_{21}] \end{bmatrix}^T [K_g] \begin{bmatrix} [I] \\ -[K_{22}]^{-1}[K_{21}] \end{bmatrix} \{u_1\}. \quad (3.37)$$

By defining the reduced stiffness matrix $[\bar{K}]$, the above reduces to,

$$\mathcal{U} = \frac{1}{2} \{u_1\}^T [\tilde{K}] \{u_1\} \quad (3.38)$$

As discussed at the beginning of this section, the ADS design variables are assigned as the horizontal and vertical deformations at all non-fixed nodes. With the integration of static condensation, design variable assignments are further restricted to non-fixed, non-condensed nodes. The procedure is now in place for calculation of strain energy and total potential energy. In summary, a flow chart of the solution procedure utilized in this chapter is shown in Figure 9.

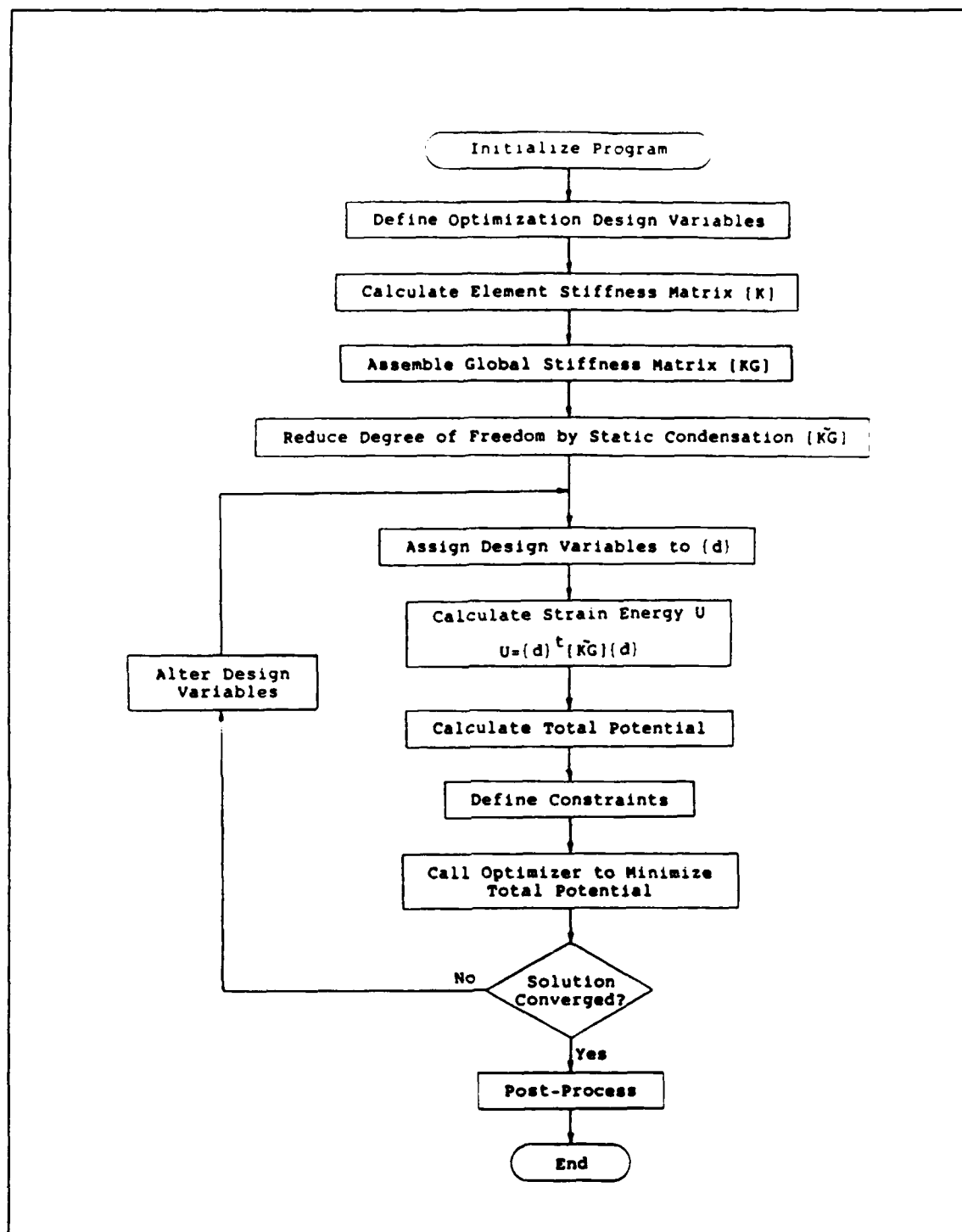


Figure 9. Finite element method applied to contact problem

IV. RESULTS AND DISCUSSION

A. PROCEDURE VALIDATIONS

1. Rayleigh-Ritz Method Results

In Chapter III an approximation technique was developed to solve the contact problem via the Rayleigh-Ritz method. As discussed, two trial functions that approximated the deformation field were selected in terms of unknown coefficients. The horizontal deformation was assumed to be:

$$u(x,y) = \sum_{n=1}^m a_n (H-y)^{(1+n)} \left(\frac{L}{2} - x \right)^2$$

The vertical deformation was assumed to be:

$$v(x,y) = \sum_{n=1}^m b_n (H-y)^2 \left(\frac{L}{2} - x \right)^{(1+n)}$$

Using the above deformation fields, theory of elasticity relationships and the definition of strain energy were employed to obtain an expression for the total potential energy of the system shown in Figure 1. Numerical minimization techniques were then employed to determine the equilibrium condition and the contact stresses.

To illustrate the application of this method, an isotropic material with the following properties was selected:

$$E = 200 \text{ GPa}$$

$$\nu = 0.3$$

$$G = 76.9 \text{ GPa}$$

As stated in Chapter II, this problem was selected for development of this technique because an analytical solution is available as a result of the work done by Hertz. It is desired to use this analytical solution to choose a roller size, load, and problem domain that can be used to accurately simulate the contact phenomenon.

Contact stresses as well as the size of the surrounding region of influence are strongly affected by the size of the contact zone. Naturally, as the size of the contact

zone increases, the load is distributed over a larger area and contact stresses decrease. The extent of the affected subsurface zone also decreases. From the analytical solution, the contact zone size is defined by the externally applied force, the material properties and the diameter of the roller [Ref. 13]. Hence for a given material, the roller size and the external load define the contact zone size and the resulting stresses.

Figure 2 defined the width of the contact zone as $2a$. Figure 3 shows the analytical solution of the contact problem. This figure shows the decrease of the normal stresses as a function of half-contact zones (a) away from the contact point. As shown, σ_x decreases more gradually than σ_z . Therefore the decay of σ_x is the limiting factor in defining the domain beyond which strain energy contributions are negligible. From Figure 3, it is estimated that the contact phenomenon can be accurately modeled by examining a region equal to approximately five half-zones ($5a$).

Since a numerical integration technique was used to perform the double integration required by Equation 3.12, the dimensions were selected for numerical convenience. Referring to Figure 8, height H and length L were selected as 1 and 2 meters, respectively. Due to the problem's symmetry, half the foundation was analyzed. This enabled the double integration to be conducted between the limits of 0 and 1. Since the foundation height H has been set to 1 m, it is desired to have this distance equal to 5 contact zones ($5a$) as described above.

Using the analytical solution, a load and roller diameter were selected that created a contact zone such that the foundation height H was equal to a distance of $5a$. The only additional restriction was that the resulting contact stresses remained within the elastic range of the material. Yield stress was assumed to be 300 MPa. The load and roller radius combination used in this study are;

$$\begin{aligned} \text{Load: } & 90 \text{ MN} \\ \text{Radius: } & 75 \text{ m} \end{aligned}$$

The values were obtained using the analytical solutions found in Reference 13. The latter dimension is unrealistic. However, as stated above, it is a result of the selection of base dimensions in the interest of numerical convenience. This model simply represents a scaled-up examination of the base material in a small region adjacent to the contact zone.

Comparisons of the approximated contact stresses with the analytical solution along the axis of symmetry are shown in Figures 10 and 11. Both figures are normalized

graphs of the stress distribution. As shown in Figure 3, the maximum stress occurs at the point of contact. As shown, this stress is equal to σ_x and σ_y at the point of contact. Figure 10 is a comparison for σ_y . This figure shows a stress distribution that closely approximates the analytical solution. Figure 11 shows the analytical and approximate stress distribution for σ_x . It is apparent that this method over approximates this stress. As stated in Chapter III, one of the benefits of this trial function is the ability to change the exponents to match analytical solutions with approximate solutions. A brief explanation of the choice of exponents used in this solution technique follows.

While selecting exponents, it must be understood that σ_x and σ_y are both functions of horizontal and vertical deformations. Therefore changing the exponent of one deformation to alter the stress in one direction will influence the behavior of the other. In the case of Figure 11, it appears that a modification is required. An increase in the exponent of the y-portion of the horizontal deformation function seems appropriate to increase the rate at which σ_x decays. However, this action will have the undesirable effect of decreasing the rate of decay of σ_y . It is possible to counter by decreasing the exponents of the vertical deformation. However, as stated in Chapter III, in order to maintain a zero stress boundary condition at $x=L/2$ and $y=H$ the exponents of all terms must be greater than or equal to 2. Thus a compromise must be reached. It is believed that since σ_y is the dominant term, priority should be placed on ensuring σ_y is as close as possible to the analytical solution. Accordingly, a decision was made to accept the over estimation of σ_x as shown in Figure 11. In this case, the estimation of σ_x is conservative.

The contours of the Rayleigh-Ritz solution are shown in Figures 12 through 15. It has been determined that this method can accurately predict contact stresses resulting from line contact between a roller and flat plane. Table 1 compares the approximated contact stresses and the analytical results at the point of contact.

Table 1. RAYLEIGH-RITZ RESULTS AT CONTACT POINT

	Current Model	Analytical Solution
σ_x (MPa)	285.6	289.7
σ_y (MPa)	301.9	289.7

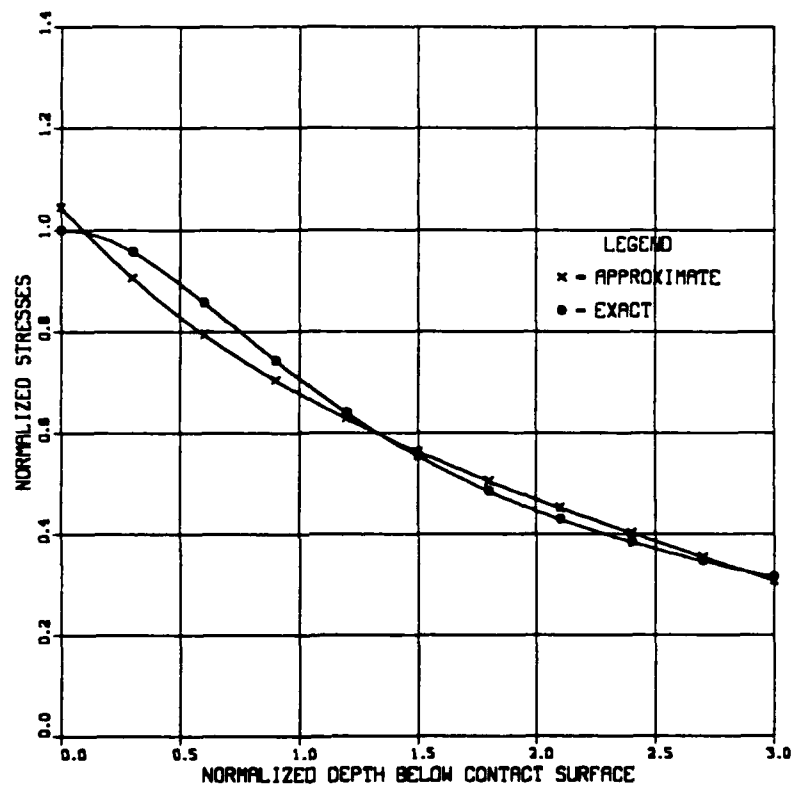


Figure 10. Comparison of σ_y in a roller contact problem

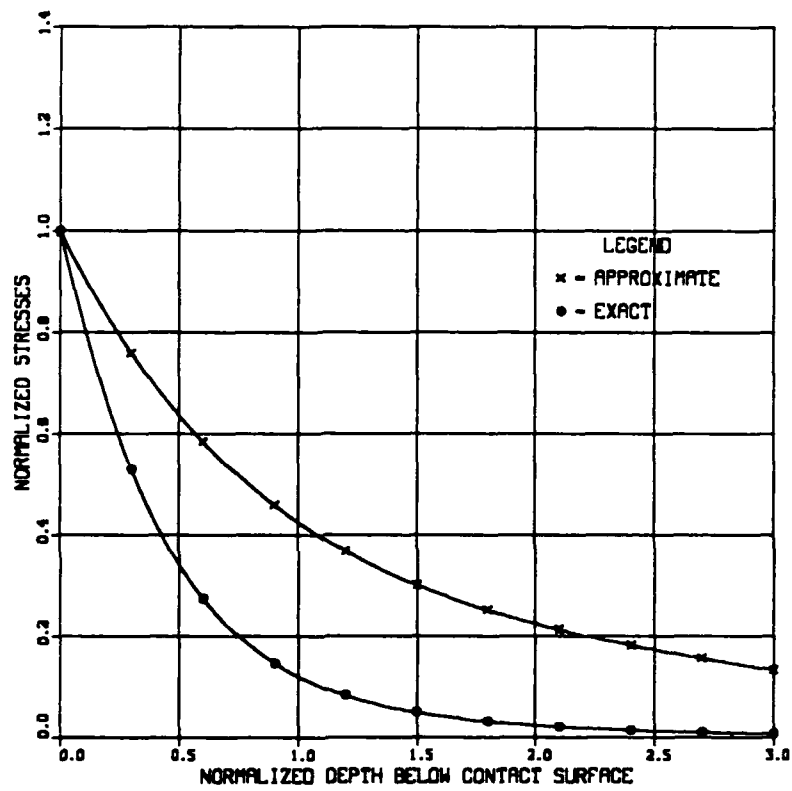


Figure 11. Comparison of σ_z in a roller contact problem

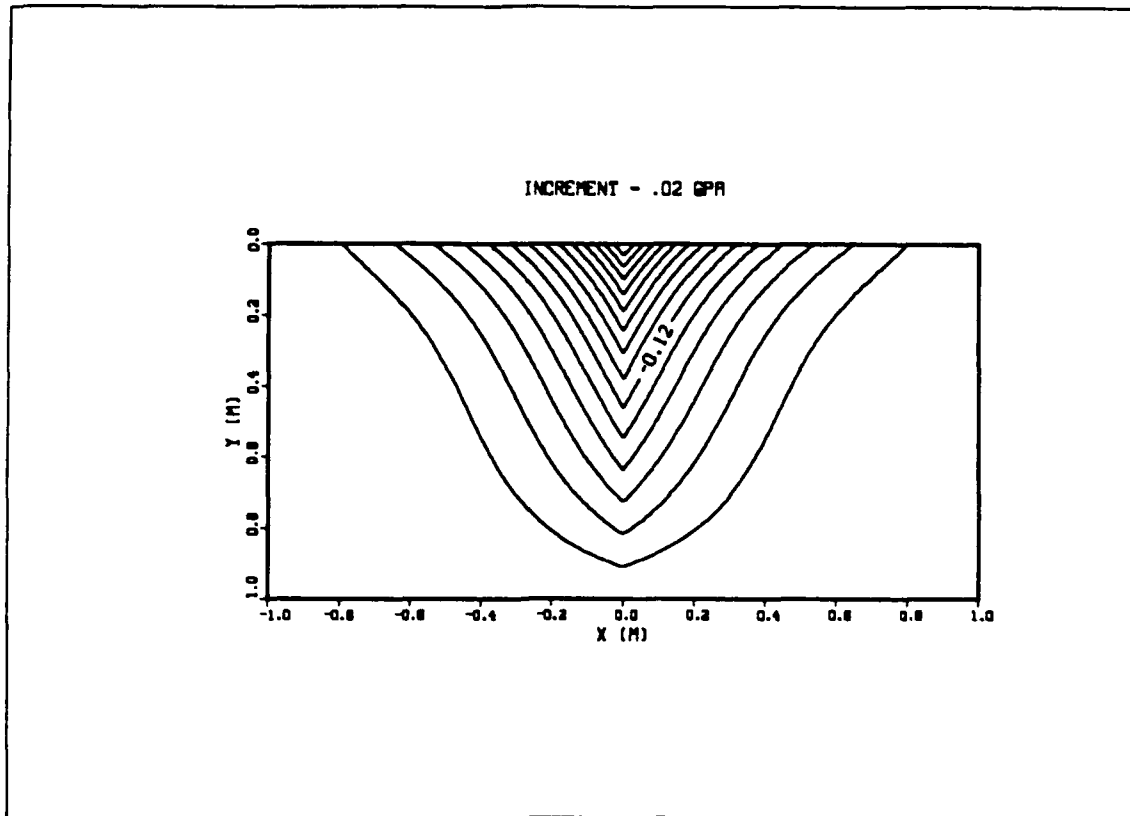


Figure 12. Stress contour of σ_y from Rayleigh-Ritz method

2. Finite Element Method Results

In Chapter III, an approximation method was developed to solve the contact problem using the finite element method. A method of calculating a system's strain energy and the total potential energy was investigated. In addition, the use of static condensation to improve optimization efficiency was described. As discussed, the numerical minimization techniques were again utilized to determine the equilibrium position. A means of employing these techniques to evaluate the contact phenomenon was introduced. In this section, a simple contact problem will be investigated to validate the algorithms used to calculate strain energy and those used to implement static condensation. With confidence in these algorithms, the more complex roller-foundation problem will be examined.

a. Two Thin Plates in Contact

The procedure developed was first validated on a simple contact problem the solution of which was known. In this example, two thin bodies in plane stress were

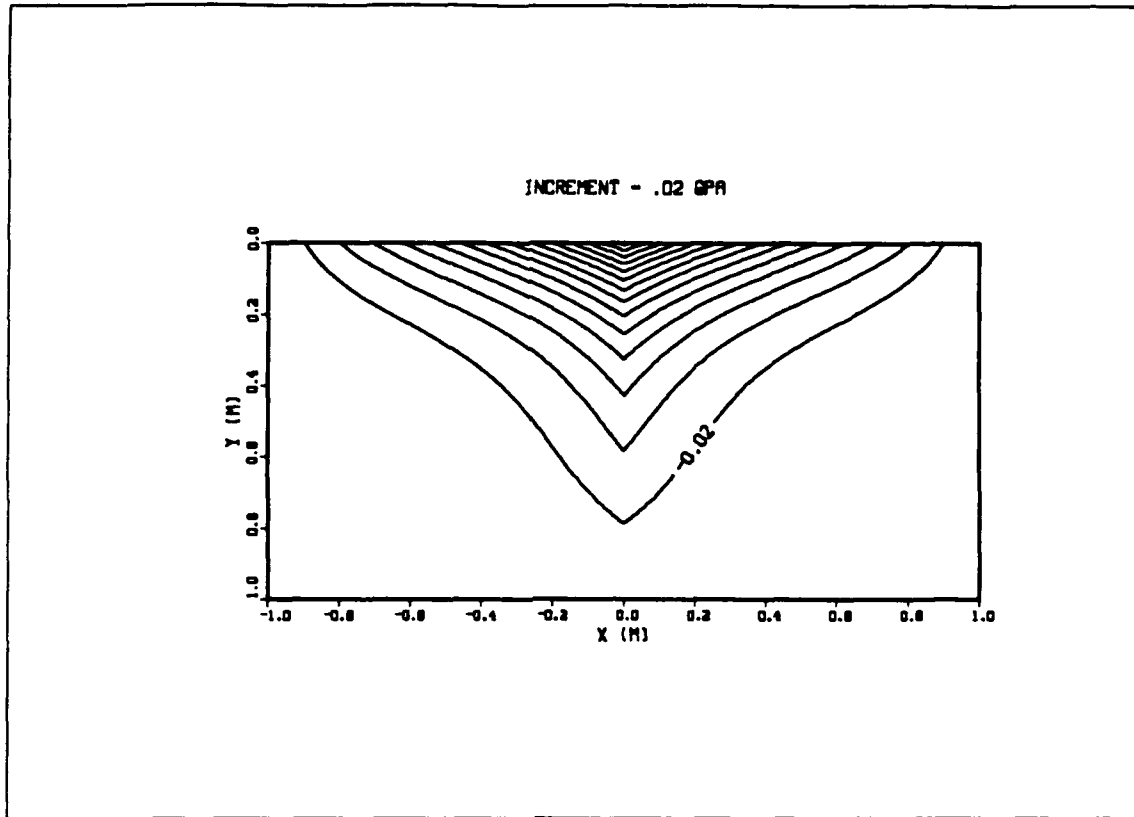


Figure 13. Stress contour of σ_x from Rayleigh-Ritz method

studied. As shown in Figure 16, one body, restrained on one edge and subjected to a horizontal load, comes in contact with a second body rigidly supported on three sides. The finite element model developed to solve this problem is composed of 14 linear triangular elements as shown in Figure 17. The objective of the fortran program developed to solve this problem was to calculate the total potential energy of the system using the finite element technique and the method of static condensation. With this accomplished, the equilibrium position can then be found via the augmented Lagrange multiplier method.

The objective function for this problem is the total potential energy, Equation 3.14. Referring to Figure 16 and 17 the constraints imposed on the system are expressed as:

$$u_8 \leq 0.005 + u_{11}$$

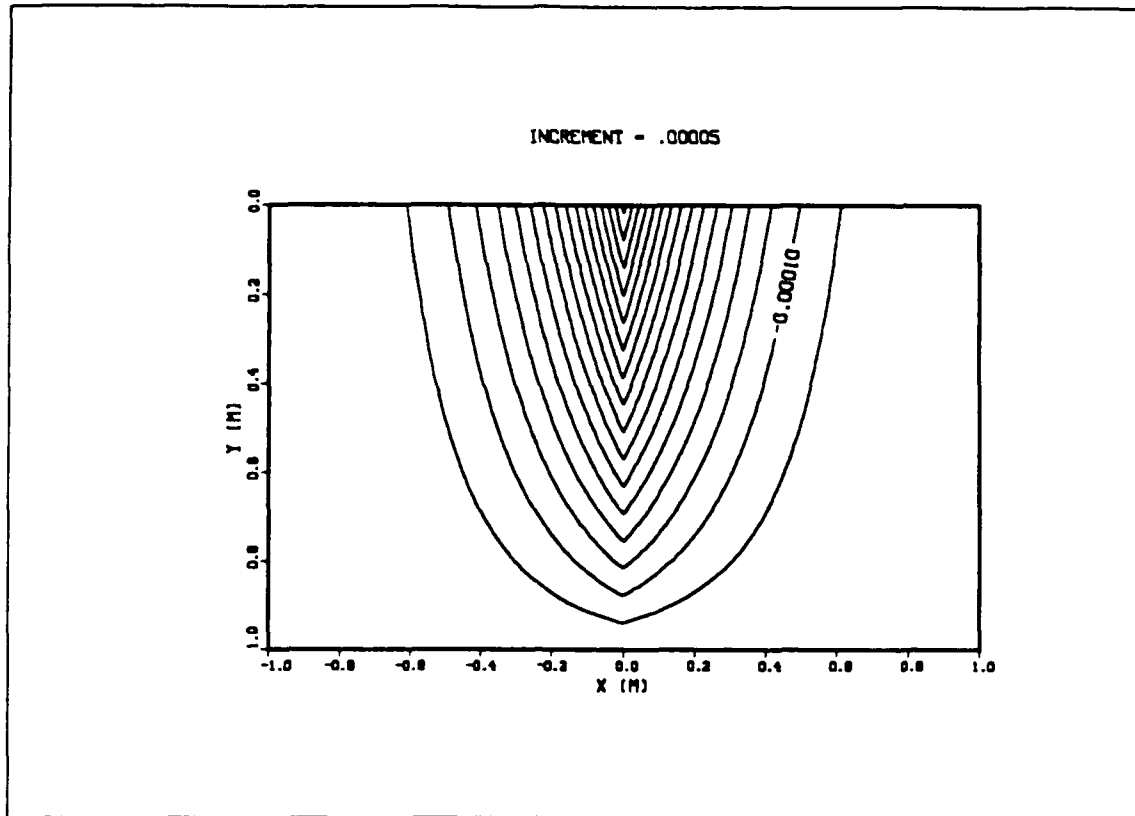


Figure 14. Strain contour of ϵ_y from Rayleigh-Ritz method

$$u_i \leq 0.005 + u_{12}$$

where u represents the horizontal deformation of node i .

As shown in Figure 17, seventeen nodes were used to model the system. Each node has been assigned horizontal and vertical deformation variables. Accordingly, the degree of freedom for this system is twice the number of nodes. As discussed in Chapter III, static condensation requires the identification of essential nodes and non-essential nodes. Essential nodes are those nodes where ADS design variables are assigned and boundary conditions are applied. Referring to Figure 17, node 3 is the point of load application and must be assigned a design variable. Nodes 8, 9, 11, and 12 are assigned design variables in order to define the constraint equations described above. After eliminating all fixed nodes from consideration, nodes 2, 5, and 6 are the only candidates for condensation. As discussed in Chapter III, the global stiffness ma-

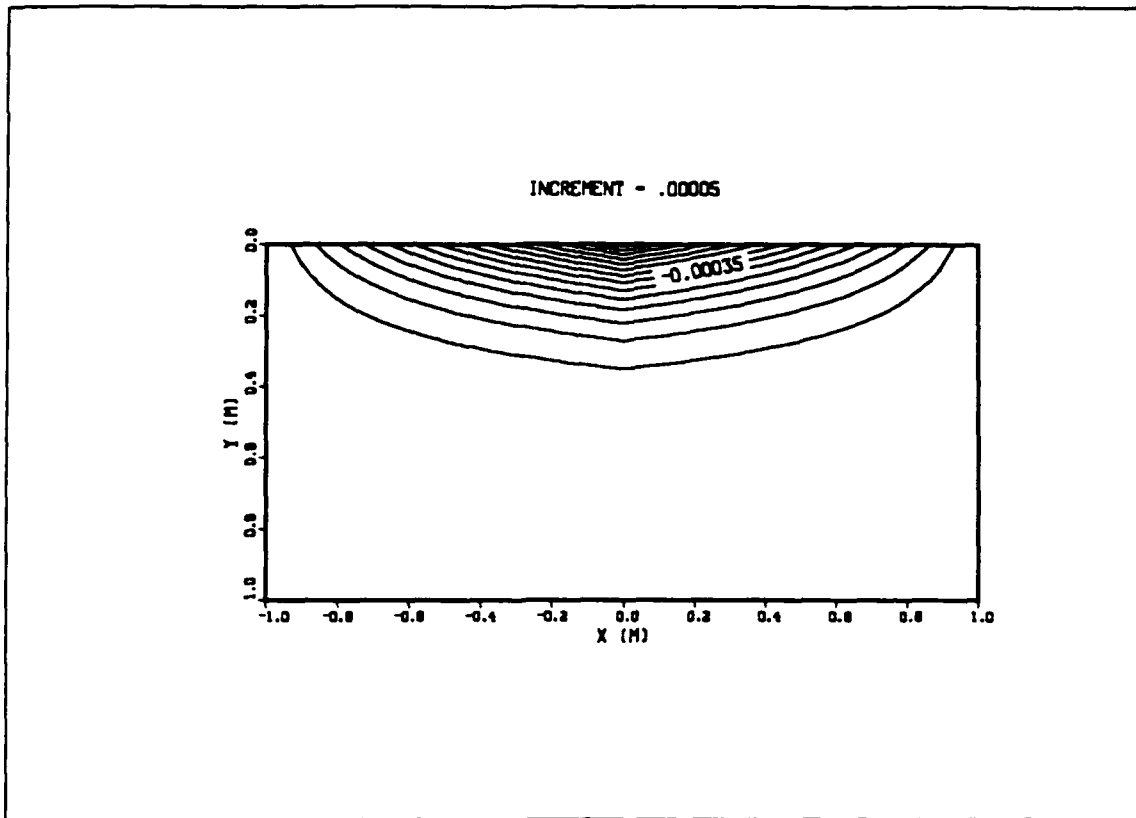


Figure 15. Strain Contour ϵ_x from Rayleigh-Ritz method

trix is rearranged according to Equation 3.34. For this problem, the vector containing the non-essential nodal information, u_2 , is arranged as follows:

$$\{u_2\}^T = \{u_2 \ v_2 \ u_5 \ v_5 \ u_6 \ v_6\}$$

where u_i and v_i represent the horizontal and vertical deformation of node i , respectively. Strain energy and total potential energy were calculated according to Equations 3.38 and 3.14. The latter was minimized using the augmented Lagrange multiplier method described in Chapter II.

The solution obtained from this simple problem were compared with the results obtained from Y.W. Kwon and J.E. Akin [Ref. 15] and are shown in Table 2. The solutions were in agreement. It was concluded that a satisfactory procedure was in place to solve the more complex roller-foundation problem.

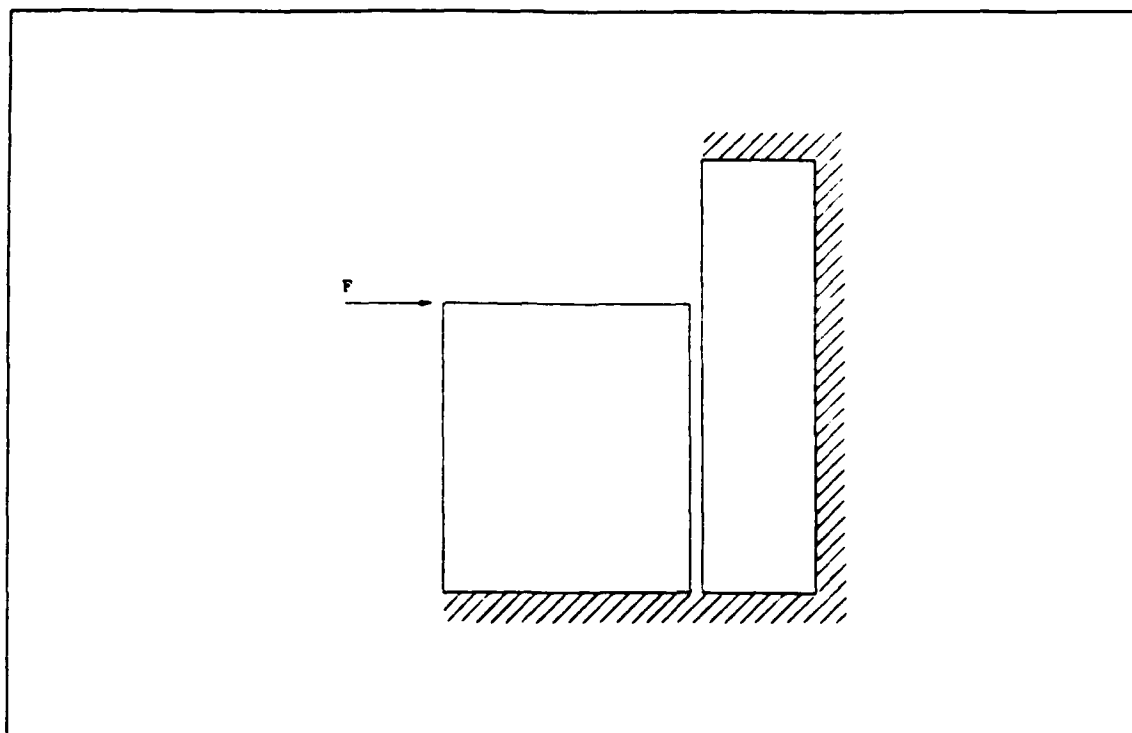


Figure 16. Two thin plates in contact

Table 2. FINITE ELEMENT RESULTS: TWO PLATES IN CONTACT

Load (N)	Deformation	Current Model	Reference 15
1.0×10^5		No Contact	No Contact
1.0×10^6	u_9	$.503 \times 10^{-2}$	$.503 \times 10^{-2}$
	u_{12}	$.336 \times 10^{-4}$	$.319 \times 10^{-4}$
1.0×10^7	u_9	$.702 \times 10^{-2}$	$.734 \times 10^{-2}$
	u_{12}	$.201 \times 10^{-2}$	$.235 \times 10^{-2}$

b. Roller-Foundation Contact Problem

A finite element grid composed of 512 linear triangular elements was constructed to model the roller-foundation assembly shown in Figure 1. Because of the symmetry of the problem, one-half of the foundation was modeled. A refined mesh was constructed in the vicinity of the point of contact. The mesh is shown in Figure 18 where the origin represents the point of contact. The domain dimensions are similar to

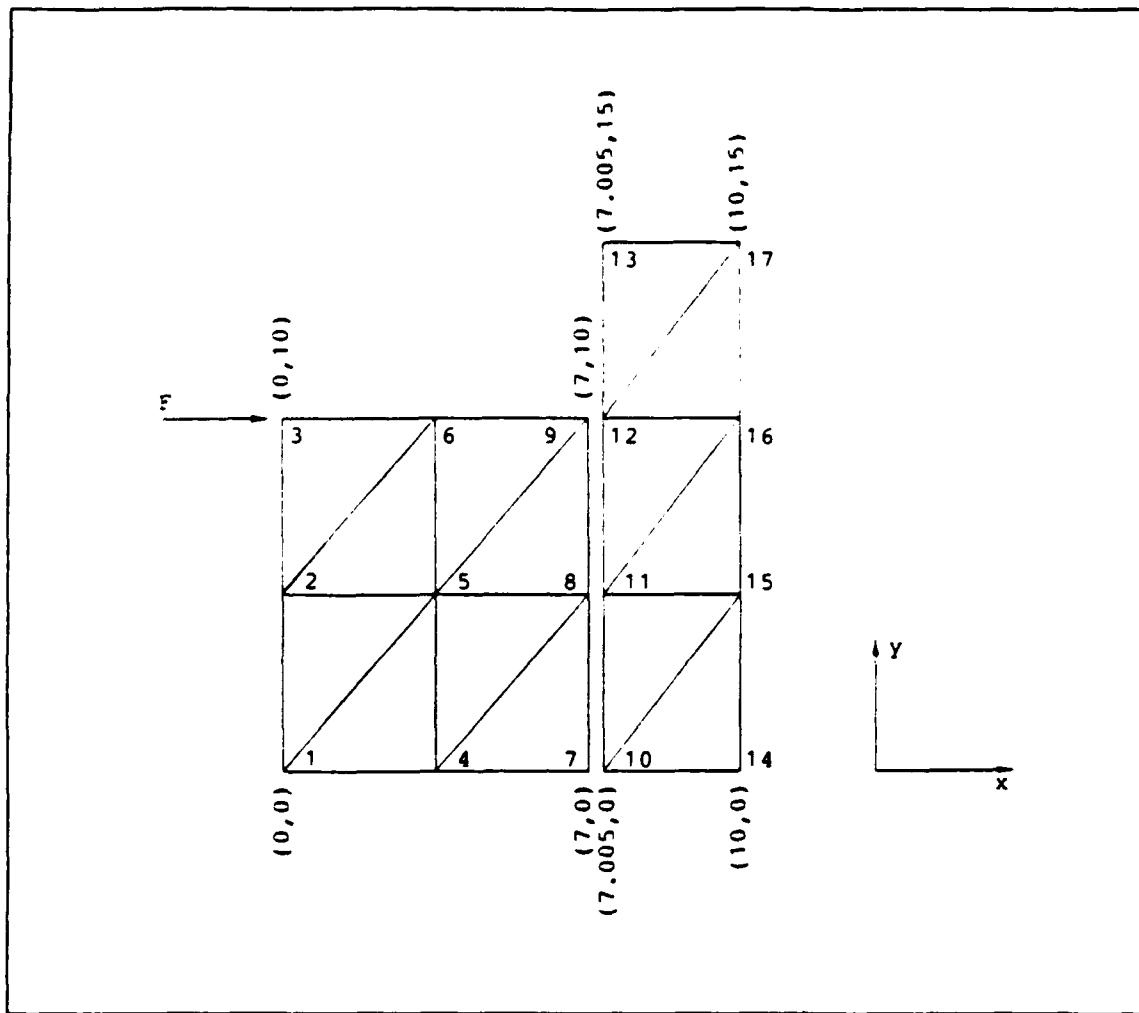


Figure 17. Finite element mesh for two plates in contact

those chosen in the Rayleigh-Ritz method discussed in Part A of this chapter. The roller radius was chosen as 75 meters and the half-domain dimensions are 1.40 x 1.40 meters. As discussed in Part A, these dimensions represent an analysis of the region immediately adjacent to the contact zone and are a result of the local nature of the contact problem.

Constraint equations were constructed according to the discussion of Chapter II Part B. Boundary conditions were imposed in the following manner:

- Horizontal and vertical deformations were prohibited on the remote mesh boundaries (i.e., $u(1.40, y) = v(1.40, y) = 0$ and $u(x, 1.40) = v(x, 1.40) = 0$).
- Horizontal deformation was prohibited on the axis of symmetry (i.e., $u(0, y) = 0$).

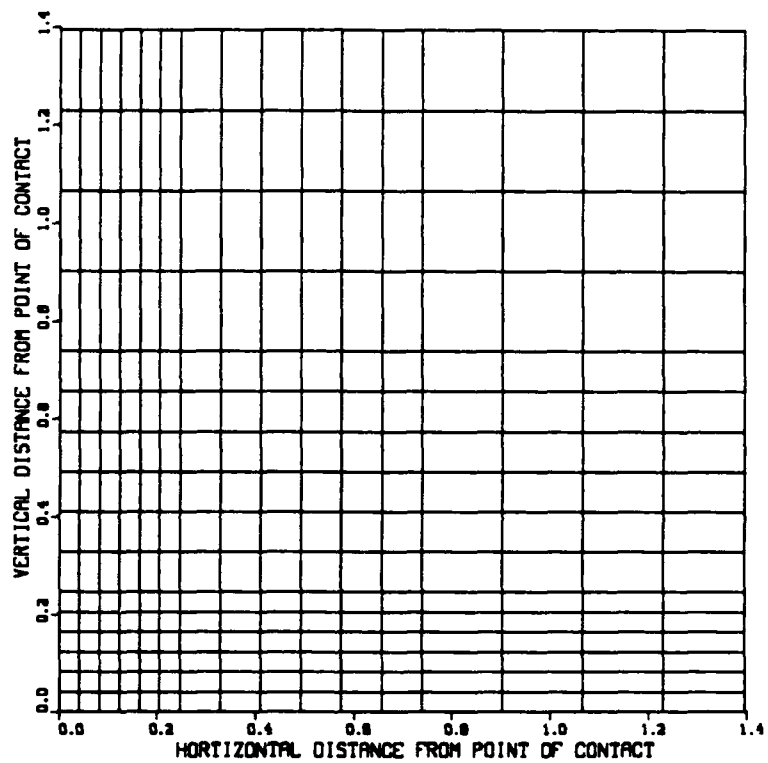


Figure 18. Finite element mesh for roller-foundation problem

Since the system has 289 nodes, the resulting 578 degrees of freedom necessitated the utilization of static condensation. Referring to the contact surface, the deformation variables that correspond to nodes on this surface are required for constraint equations. The nodes that comprise the other three borders of the domain are all subject to boundary conditions. Consequently, the interior nodes of the mesh are the nodes that are candidates for static condensation. In this model, all interior nodes were condensed. The original system was reduced from 578 to 128 degrees of freedom. After application of the boundary conditions, there were 46 possible deformations, a sufficiently small number of design variables for the optimization algorithm. One additional design variable was used to represent the distance of travel by the roller. This value is needed to calculate the work done by the roller on the bearing foundation.

As before, Equation 3.38 was used to calculate the system's strain energy. Following calculation and the subsequent minimization of the total potential energy, a post-processing procedure was followed to determine the contact stresses. The output of the optimization routine represents the nonzero components of the $\{u_1\}$ vector. In order to calculate stresses throughout the body, the remaining deformations contained within the condensed vector $\{u_2\}$ must be determined. This vector is calculated directly using Equation 3.35. With deformations known throughout the domain, strains can be determined by applying Equation 3.27 to each element. The subsequent application of Equation 3.18 enables determination of stress for each element.

To illustrate the capability of this method, an isotropic material with the following properties was chosen:

$$E = 240 \text{ GPa}$$

$$\nu = 0.3$$

$$G = 92.3 \text{ GPa}$$

$$\text{Load} = 90.0 \text{ MPa}$$

Figure 19 shows the deformation resulting from the loading. For clarity, the deformations have been magnified 100 times their original values. Comparisons of the stress distributions with the analytical solution along the axis of symmetry are shown in Figures 20 and 21. These figures are similar to Figures 10 and 11 and represent normalized versions of contact stresses. As shown in these figures, this method is a good approximation of the stress distribution in the foundation of a loaded roller bearing. If the mesh

was more refined near the contact zone and the domain extended further, the agreement between the numerical and analytical solutions would be better. Figures 22 and 23 represent normal stress contours of this problem. Figures 24 and 25 show normal strains. Table 3 shows a comparison of the results of this model and the analytical solution at a selected element in the region of contact.

Table 3. COMPARISON OF STRESSES NEAR THE POINT OF CONTACT

	FEM Solution	Analytical Solution
σ_x (MPa) at $x = 0.0137$, $y = 0.0273$	281.3	272.0
σ_y (MPa) at $x = 0.0137$, $y = 0.0273$	315.7	313.8

B. APPLICATION

The preceding section illustrated that the contact problem can be accurately simulated using the methods developed in Chapter III. It is the objective of this section to show how this approach can be applied to a contact problem in a composite plate subjected to low-velocity impact.

A multi-ply laminate model has been constructed to investigate the response of composite materials to low velocity impact. It has been found that composite bodies subject to impact damage commonly fail due to delamination. Sandwich composites are currently being considered for use as turbine blades. It would be beneficial to acquire an understanding of the behavior of sandwich materials to impact damage.

In order to accomplish this task, a clamped composite beam similar to the one depicted in Figure 26 has been modeled. The beam length is 25 cm. Beam thickness is 2.5 cm. Because of symmetry, half the beam was modeled with 256 bilinear elements. As shown in Figure 27, the mesh is refined near the point of contact, the origin of the mesh.

The major assumptions of this model are that the beam is in a condition of plane strain and that the dynamic effect of the impact can be neglected. Reference 10 approximated the loading resulting from low velocity impact as a sinusoid. In this study, the peak load will be examined to study the maximum normal and shear stresses. Accordingly, the stress distributions obtained from this study will represent a 'snap-shot' in time of the response of the body at the instant of maximum loading.

The finite element program developed to solve this problem is sufficiently flexible to alter the material stiffness matrix $[D]$ shown in Equation 3.18 during construction of the

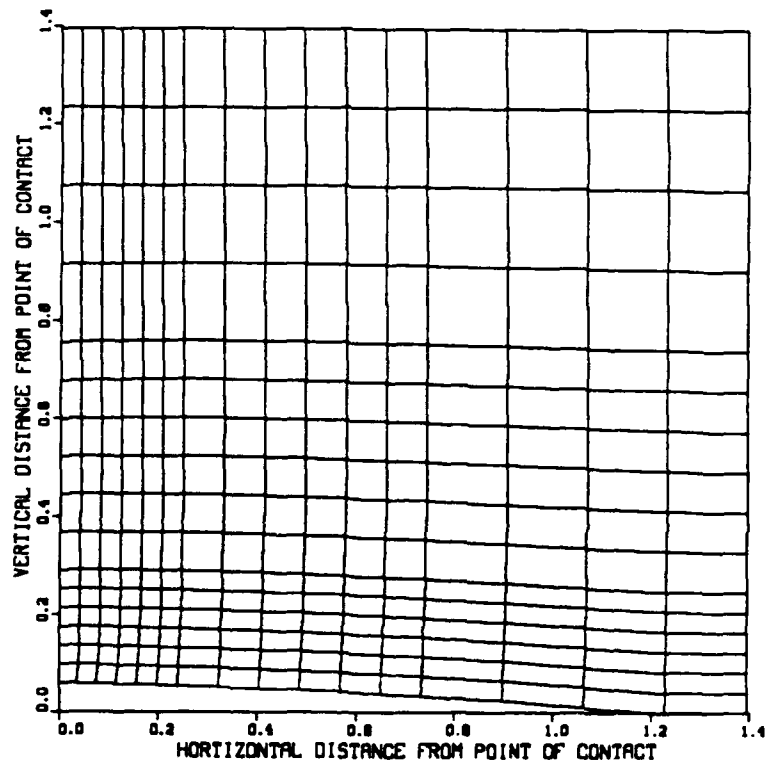


Figure 19. Deformed finite element solution: deformation magnified 100 times

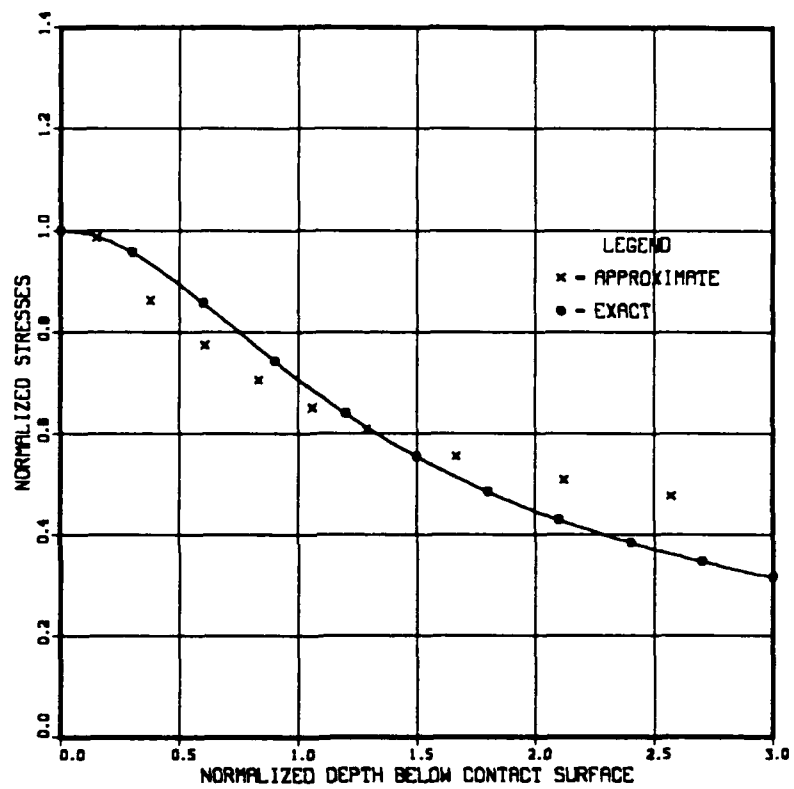


Figure 20. Analytical solution vs. approximate σ_y from finite element results

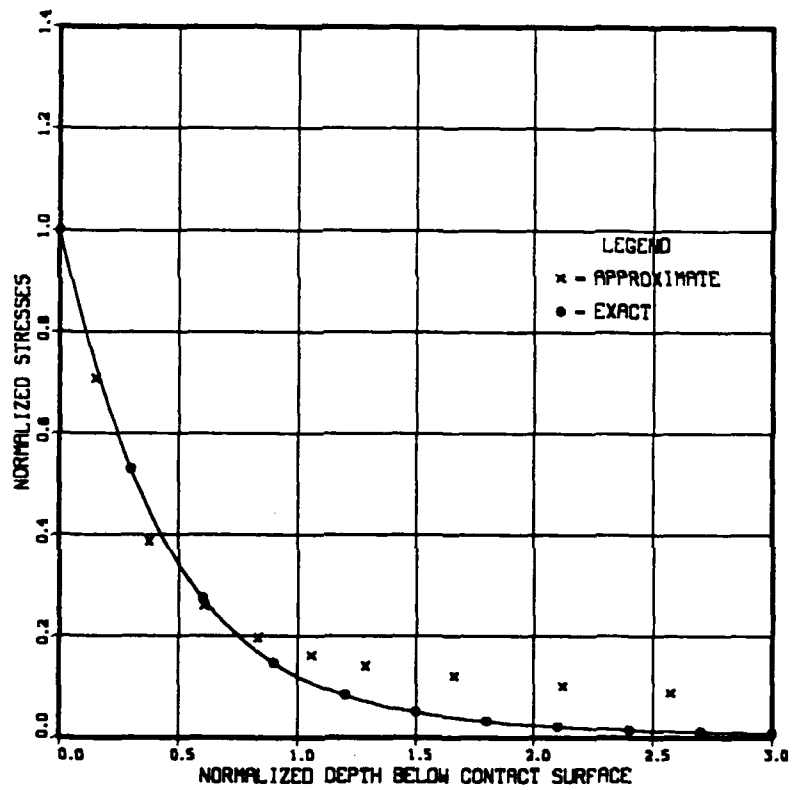


Figure 21. Analytical solution vs. approximate σ_x from finite element results

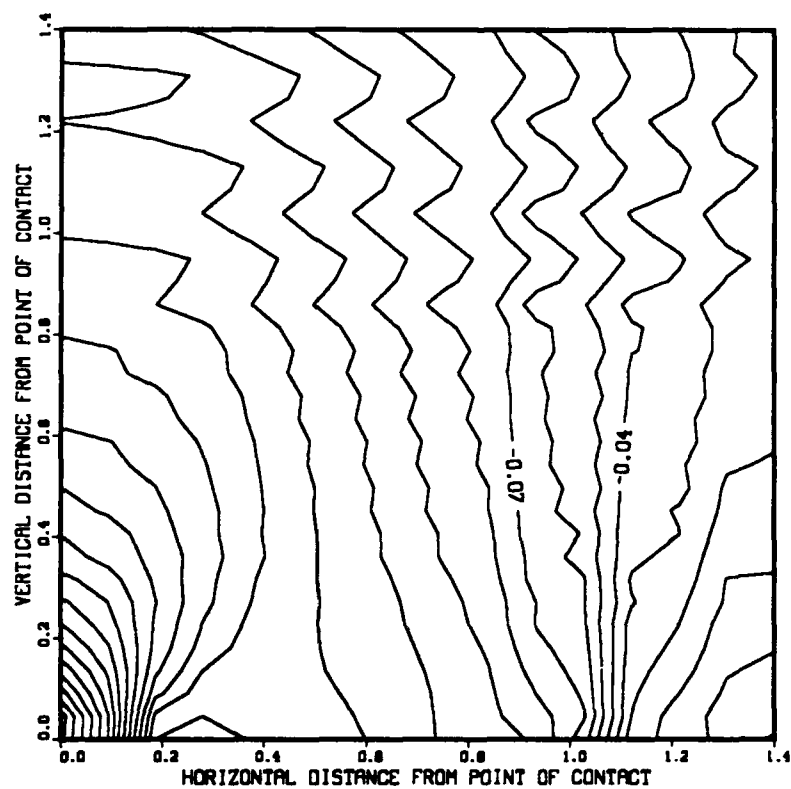


Figure 22. Stress contour σ_y from finite element results (increment 0.01 GPa)

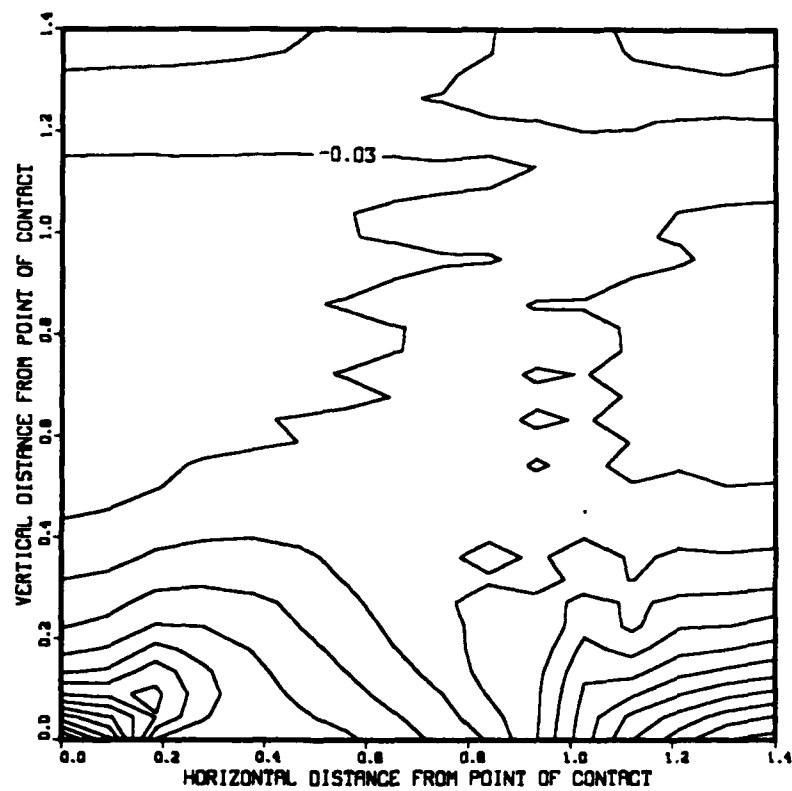


Figure 23. Stress contour σ_x from finite element results (increment 0.02 GPa)

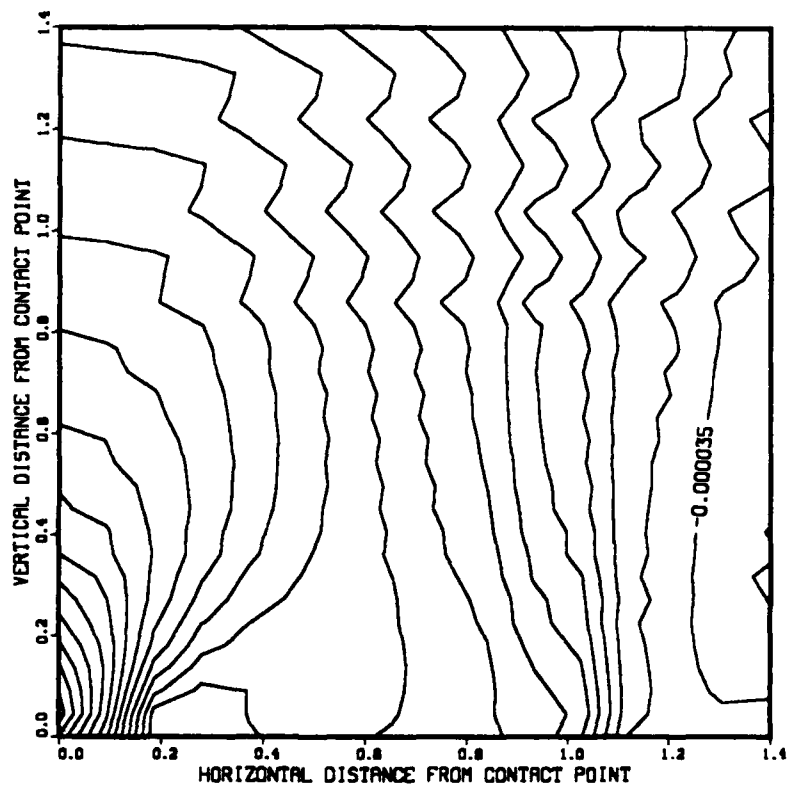


Figure 24. Strain contour ϵ_y from finite element results (increment 0.000035)

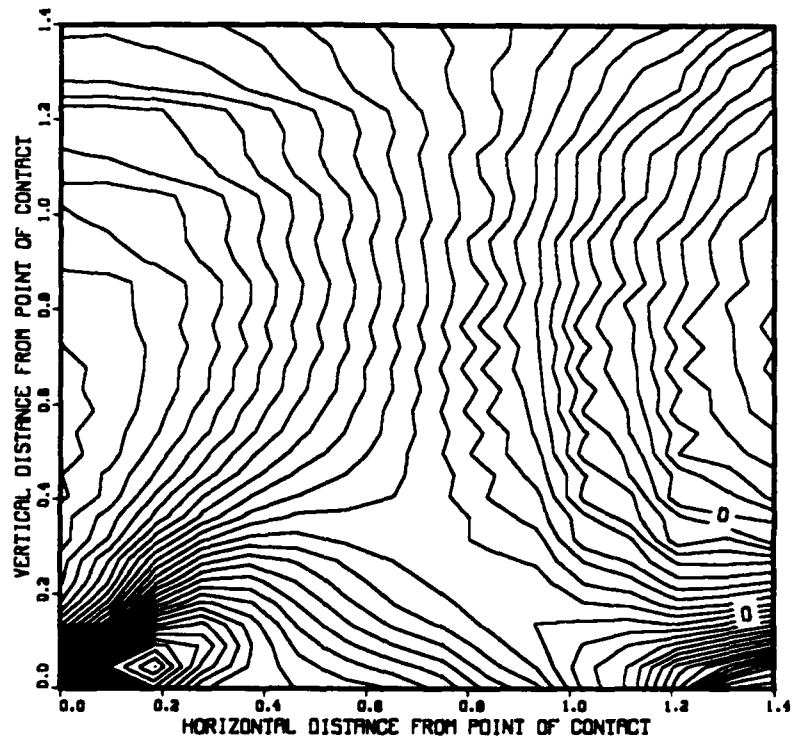


Figure 25. Strain contour ϵ_x from finite element results (increment 0.00001)

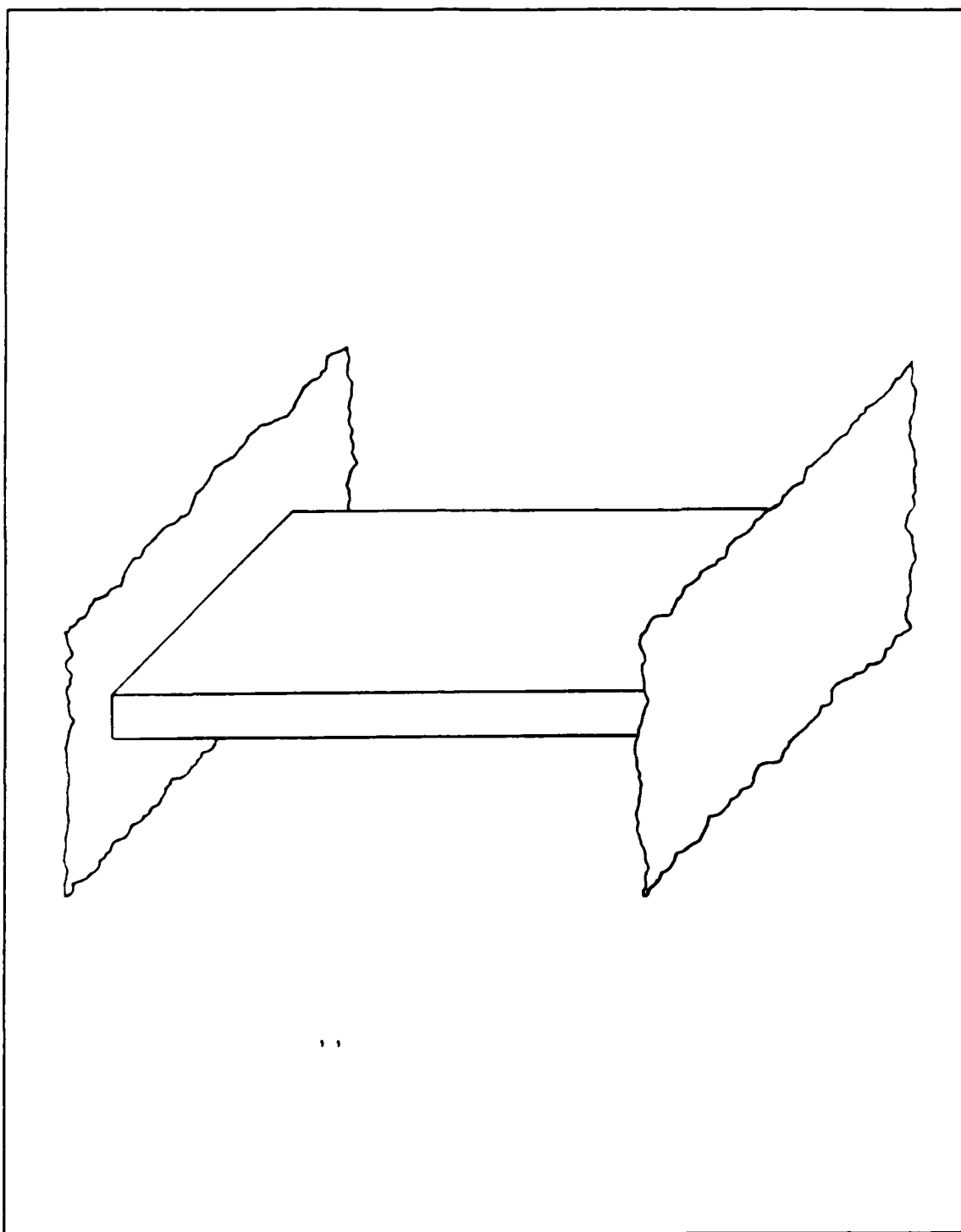


Figure 26. Clamped composite beam

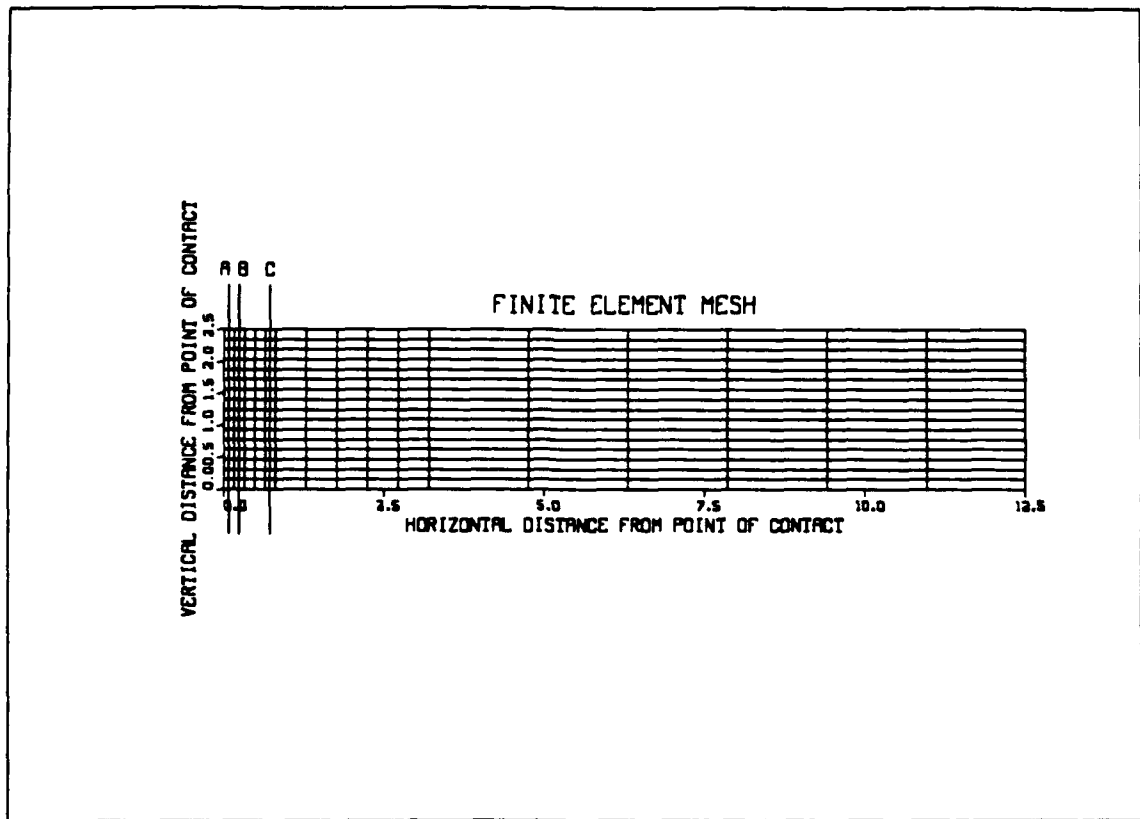


Figure 27. Finite element mesh for clamped beam model

finite element global stiffness matrix. Therefore by defining the layup for the laminate, the lamina stiffness matrices can be varied from element to element to accurately model the behavior of the body. This enables a variety of laminate layups and lamina thicknesses to be studied.

The sandwich materials used in this study are composed of an isotropic interior material and orthotropic exterior laminae. Since a condition of plane strain was assumed, the isotropic material stiffness matrix is given by Equation 3.19a. For the orthotropic exterior laminae, the material stiffness matrix is given by Equation 4.1 [Ref. 16].

$$[D] = \begin{bmatrix} \frac{1 - v_{23}v_{32}}{E_2 E_3 T} & \frac{v_{12} + v_{32}v_{13}}{E_1 E_3 T} & 0 \\ \frac{v_{12} + v_{32}v_{13}}{E_1 E_3 T} & \frac{1 - v_{13}v_{31}}{E_1 E_3 T} & 0 \\ 0 & 0 & G_{12} \end{bmatrix} \quad (4.1)$$

where,

$$T = \frac{1 - v_{12}v_{21} - v_{23}v_{32} - v_{31}v_{13} - 2v_{21}v_{32}v_{13}}{E_1 E_2 E_3}$$

E_i = Young's Modulus in i^{th} direction

v = Poisson's ratio for lateral contraction in j^{th} direction resulting from loading in the i^{th} direction

The derivation of the total potential energy calculation in Chapter III, Part B was done using linear triangular elements. Since bilinear elements were used in this model, calculation of the element stiffness matrix was more computationally intensive. Individual entries of the element stiffness matrix were obtained from Reference 17. Otherwise, the calculation of total potential energy was identical to the procedure outlined in Chapter III.

There were two groups of boundary conditions applied to the problem. Along the clamped edge, deformation was prohibited. In addition, horizontal deformation was prohibited along the axis of symmetry. As before, the application of static condensation requires the identification of essential nodes the information of which is contained within the $\{u_i\}$ vector. In addition to the essential nodes associated with the above boundary conditions, the nodes along the contact surface are needed for the constraint equations. All other nodes were condensed out.

To illustrate this application of problem solving, sandwich material with the following properties were studied:

Exterior Laminae

$$E_{11} = 170 \text{ GPa}$$

$$E_{22} = 11.8 \text{ GPa}$$

$$G_{12} = 5.2 \text{ GPa}$$

$$v_{12} = 0.33$$

Isotropic Core

$E = 2.24 \text{ GPa}$

$G = 0.84 \text{ GPa}$

$\nu = 0.35$

The beam was loaded by contact with a 10 cm radius ball. The transmitted force was 250 N. Some unexpected trends were observed in the equilibrium position determined by the optimizer. By examining the deformations along the axis of symmetry, a gradually decreasing trend in deformation moving away from the point of contact was interrupted in lamina of significantly decreased stiffness. It is believed that this difficulty resulted from an inability of the optimization routine to approximate deformations through regions containing very different orders of strain energy. In spite of these difficulties, some critical information was obtained from this program. As discussed in the beginning of this study, one of the greatest difficulties of the contact problem is the determination of the size of the contact zone. Fortunately, the size of the contact zone can be readily determined by examining the output from the constraint equations. By comparing the ball radius (r) and the distance between the ball center and the node (r'), it can be determined if a node is in contact. This condition is illustrated in Figure 28. The distance r' to the i_n node is given by the equation:

$$r' = \sqrt{(r - \delta + v_i)^2 + x_i^2}$$

If r' is greater than r , the node is not in contact with the body.

With the extent of the contact zone known, the solution to this problem was obtained by applying the contact boundary condition to a direct finite element program. Since the validity of the optimization program was in question, this method was applied using a 0-90-0 layup similar to one used in a study conducted by Sun and Rechak [Ref. 10]. The solution obtained from the current approach was very close to the other results.

With confidence in the procedure, it was desired to examine the behavior of this model to various layups. The objective was to illustrate how this solution technique can be used for meaningful research. The study conducted by Sun and Rechak analyzed methods of reducing the likelihood of composite failure due to delamination. Of particular concern is the magnitude of shear stress distribution and tensile stress in the y-direction, the two predominant causes of delamination failure. Using materials with the

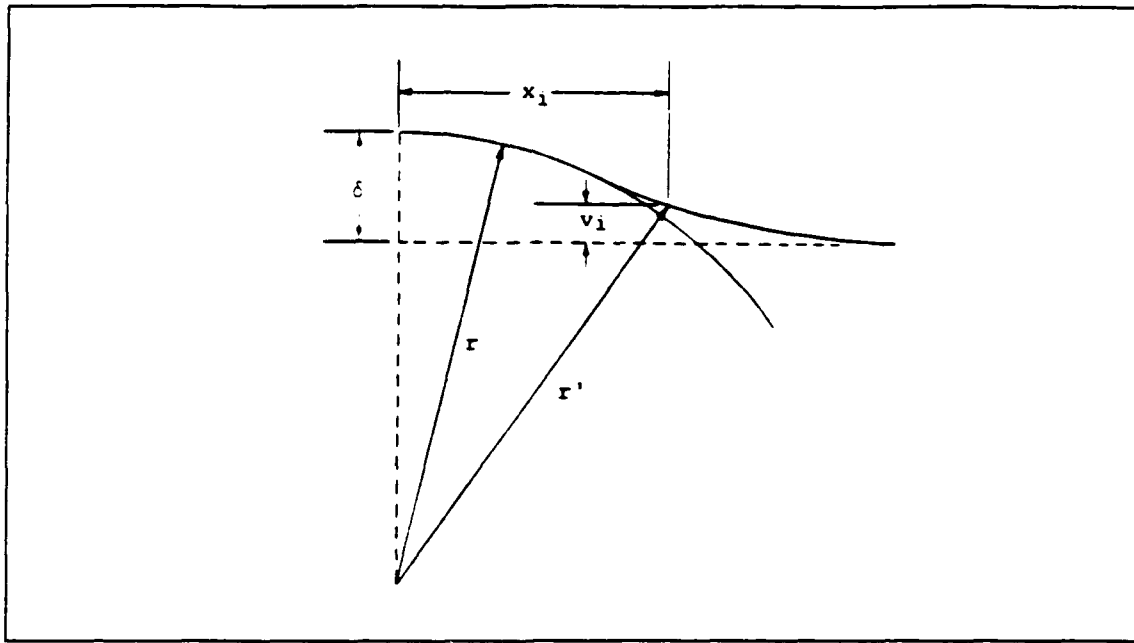


Figure 28. Determination of nodal contact

properties outlined above, a sandwich composite beam with outer fibers aligned to 0 degrees was first studied. Since the finite element model is composed of 16 layers, the beams studied will be described with the number of finite element layers in parenthesis following the layer description. For example, a 0(3)-ISO(10)-0(3) beam is composed of 10 isotropic core layers within 3 layers of material with the fibers oriented at 0 degrees on the top and bottom of the beam.

Three symmetric layups of varying core thickness were initially studied. The beams have the following designations: 0(3)-ISO(10)-0(3), 0(4)-ISO(8)-0(4), and 0(5)-ISO(6)-0(5). Figure 29 shows the deformed 0(3)-ISO(10)-0(3) beam with deformations magnified 100 times. Stress contours for this beam are shown in Figures 30, 31, and 32. Figure 30 shows the shear stress contour for the loaded condition. This stress is of particular concern since delamination, a common failure mode for composites, is commonly initiated by high shear stresses or tensile transverse normal stresses. As the figure shows, a very high stress gradient is present near the contact zone. As the distance along the beam increases away from the contact zone, the magnitude of the gradient decreases until the cross sectional shear stress distribution becomes parabolic. The transverse normal stress is also concentrated around the contact zone.

Figures 33, 34, and 35 show the cross sectional shear stress distributions for the three symmetric beams described above. Three separate cross sections are shown on

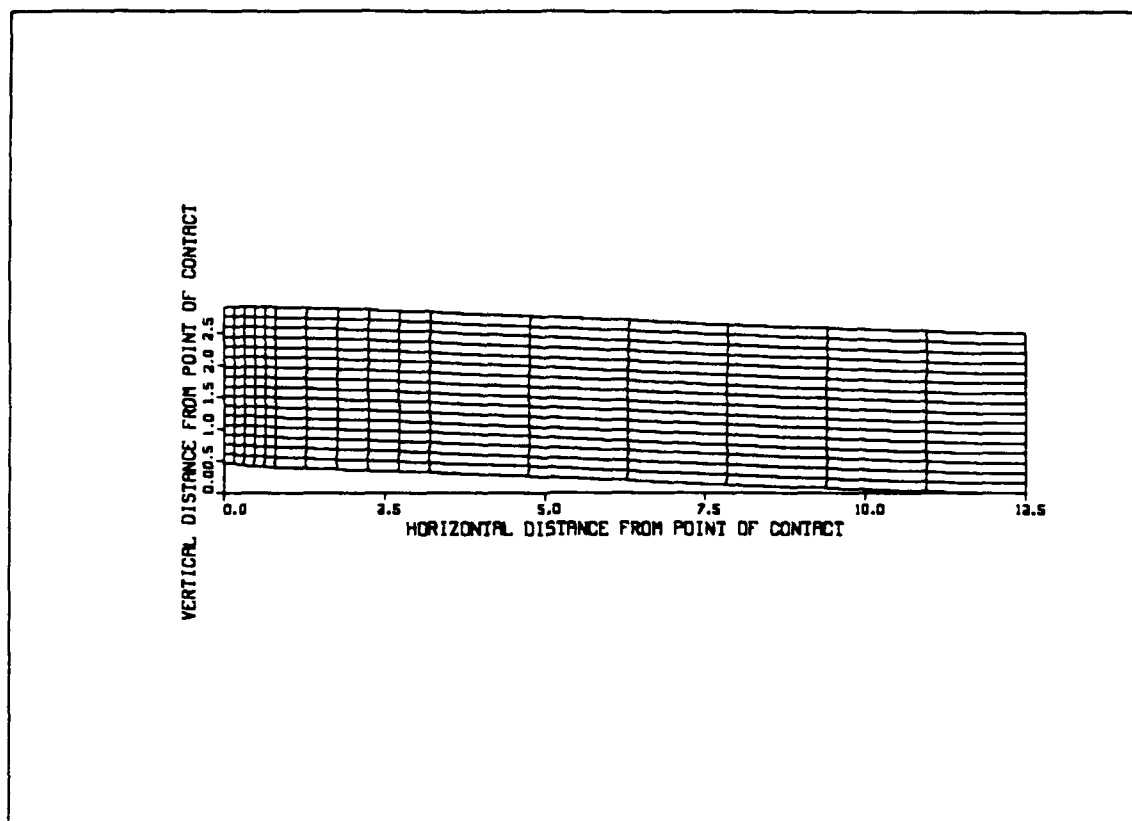


Figure 29. Loaded beam: deformation magnified 100 times

each graph, the locations of which are indicated in Figure 27. The vertical dashed lines on each graph identify the lamina interfaces. These figures show that all significant activity is confined to the lamina closest to the contact zone. It is also evident that the maximum shear stress is relatively insensitive to the core thickness. However, as the thickness of the layer closest to the contact surface increases, the shear stress transition is more gradual at the interface with the core. The result is a reduction in the shear stress at the interface for layups with thicker exterior lamina. It is also noteworthy that the maximum shear stress occurs at cross section B vice cross section A.

Figures 36, 37, and 38 are graphs for the transverse normal stress, σ_y , for the same three symmetric layups. These graphs show an increase in σ_y as the thickness of the exterior layers increases. The increased thickness of these layers produces a stronger beam, hence beam deflection and contact zone size are reduced. Accordingly, contact stresses increase. At cross section C, some tensile transverse stress is evident. As previously stated, tensile transverse stress is a potential source of delamination. As the

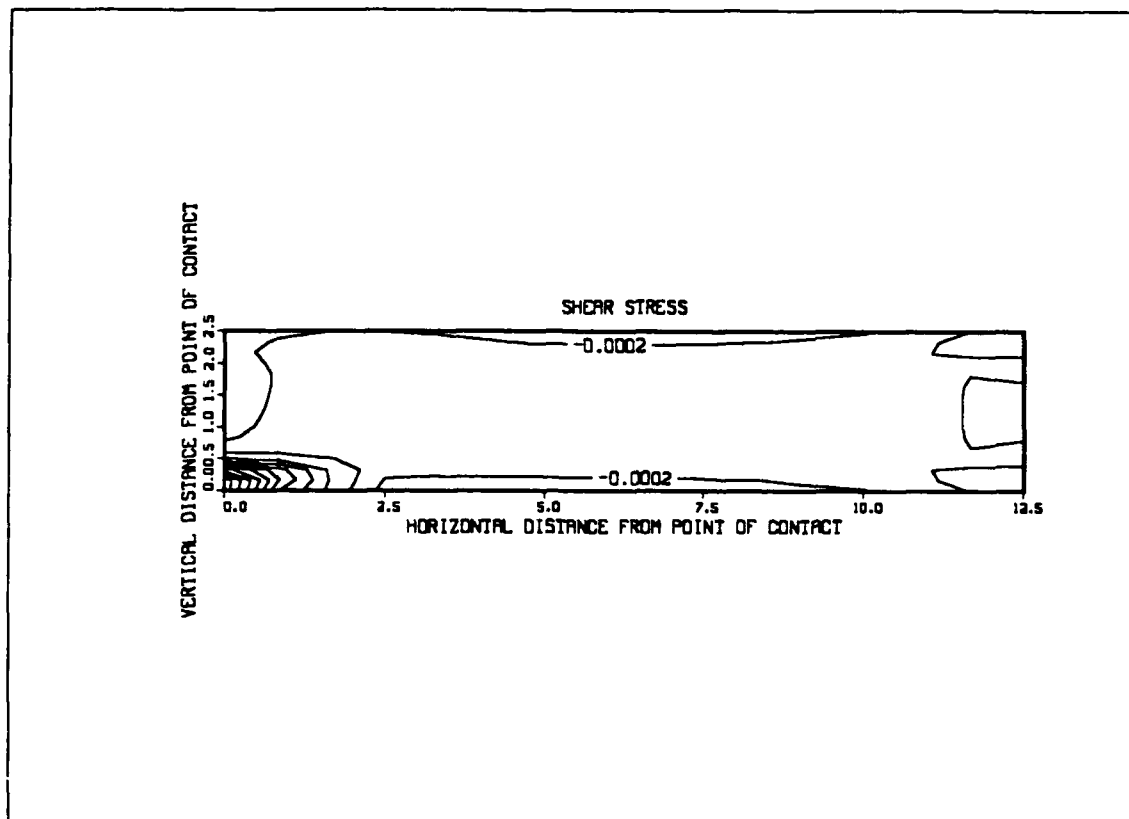


Figure 30. Stress contour: τ_{xy} for clamped beam model

thickness of the exterior layer increases, the maximum value of this stress increases. However, this stress is always compressive at the interface with the core. By comparing the magnitudes of the shear and transverse normal stresses at the interface, it would appear that if delamination was to occur at this interface, it is more likely to be caused by high shear stresses.

Comparisons of the bending stresses at cross section A are shown in Figures 39, 40, and 41. These figures show that as the thickness of the exterior layer increases, a nonlinear stress distribution intensifies in the layer closest to the contact surface. This trend would indicate that beam theory is unsuitable for estimating bending stress through this lamina. This nonlinear behavior is local to the contact zone. Figure 42 shows the counterpart for Figure 41 at cross section C. The stress distribution in the contact layer is approximately linear. Another significant observation can be made by examining the bending stress graphs. As the thickness of the exterior layer opposite to the contact layer increases, the stress distribution within this layer transforms from purely tensile

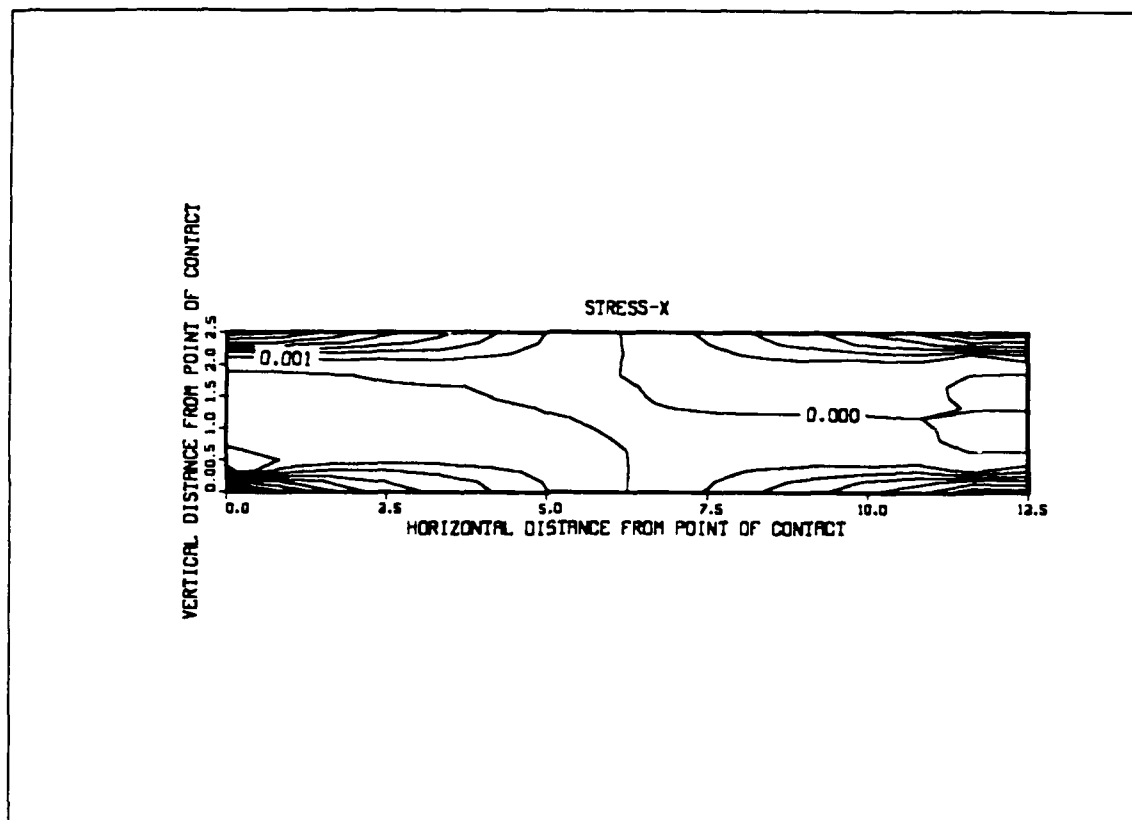


Figure 31. Stress contour: σ_x for clamped beam model

behavior to compressive-tensile behavior. This is significant because a bending crack initiated by tensile stresses tends to propagate to the core interface and cause delamination. The presence of compressive stress within this layer will tend to slow the growth of this crack toward the core.

Thus far symmetric layups have been studied. To analyze how beams with asymmetric layups respond to contact loading, two beams with the following designations were studied: 0(3)-ISO(6)-0(7) and 0(8)-ISO(6)-0(2). The first designated layer is the lamina closest to the contact surface. Figures 43 and 44 show the shear stress distributions for these two layups. As before, the maximum shear stress is relatively unaffected by the different layups. As was the case for the symmetric beams, a thicker exterior layer close to the contact zone results in a more gradual transition of shear stress into the core. The result is a lower shear stress at the interface for the 0(8)-ISO(6)-0(2) case. As seen in Figures 45 and 46, the trends for the transverse normal stress, σ_x , were the same as those found in the symmetric beams. Deflection was less for the

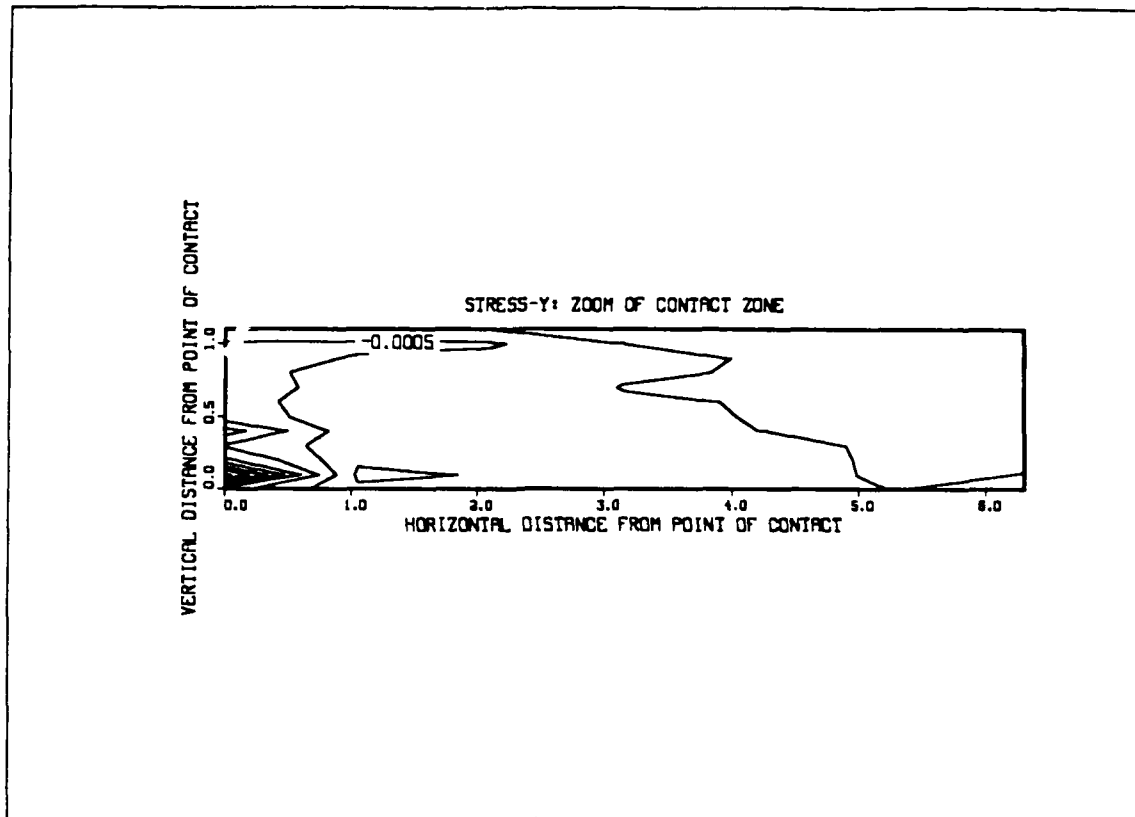


Figure 32. Stress contour: σ_y for clamped beam model (In region of contact)

0(8)-ISO(6)-0(2) case. The resulting smaller contact zone lead to higher contact stresses. As seen in the symmetric cases, an increase in the thickness of the layer closest to the contact zone resulted in an increase in the magnitude of the maximum tensile transverse stress, seen at cross section C. However, the stress at the laminate interface was always compressive.

With regard to bending stresses for these layups, Figures 47 and 48 clearly show the nonlinear behavior as the contact layer thickness increases. In addition, the thickness of the exterior layer opposite to the contact surface shows similar results as the symmetric cases. As the thickness of this layer decreases, the beam is more susceptible to a bending crack that propagates into the interface.

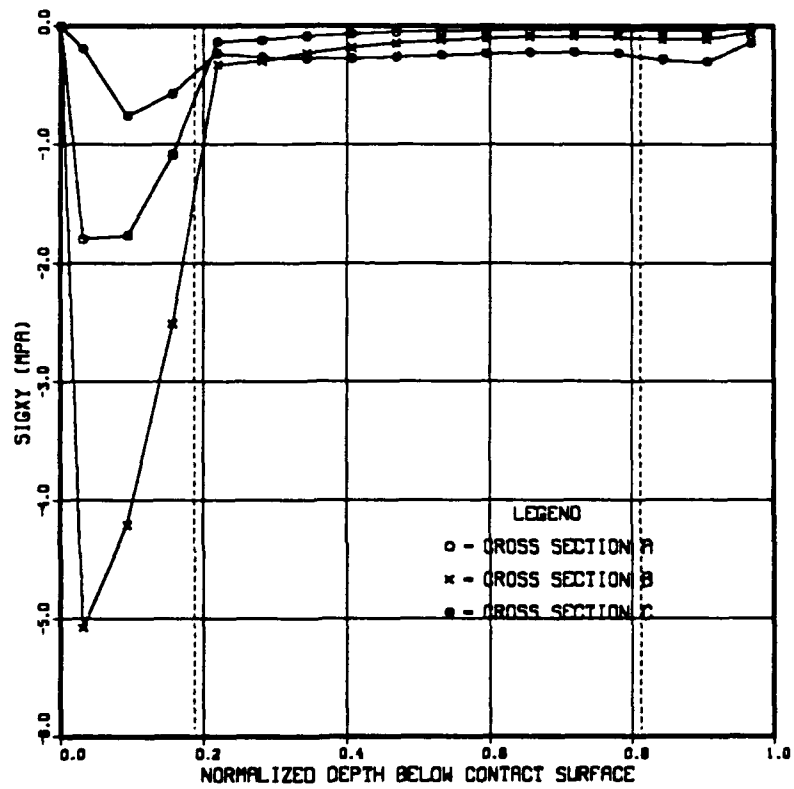


Figure 33. Stress distribution: τ_{xy} for 0(3)-ISO(10)-0(3) laminate

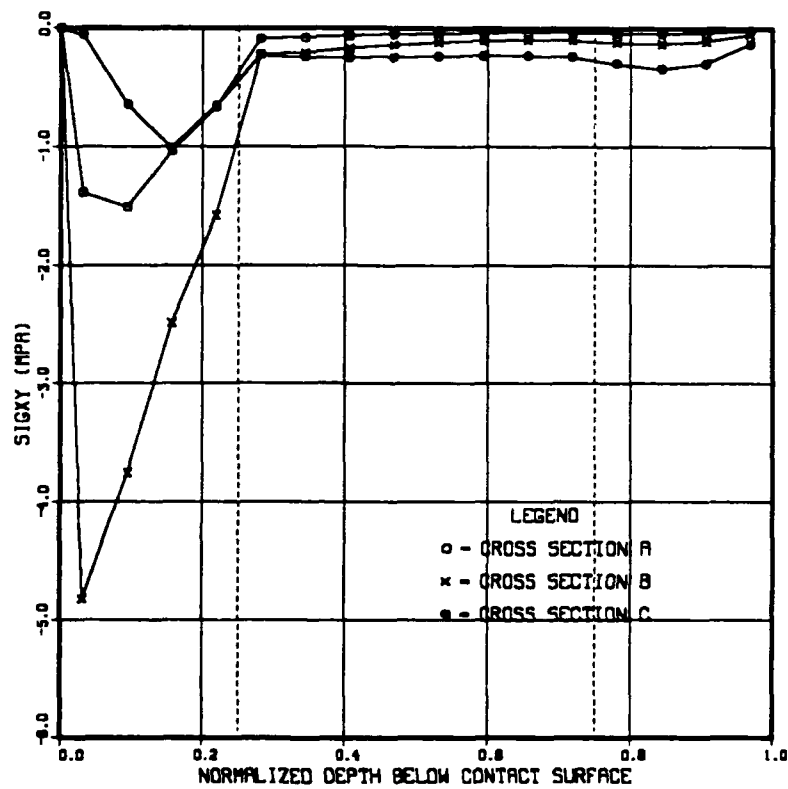


Figure 34. Stress distribution: τ_{xy} for 0(4)-ISO(8)-0(4) laminate

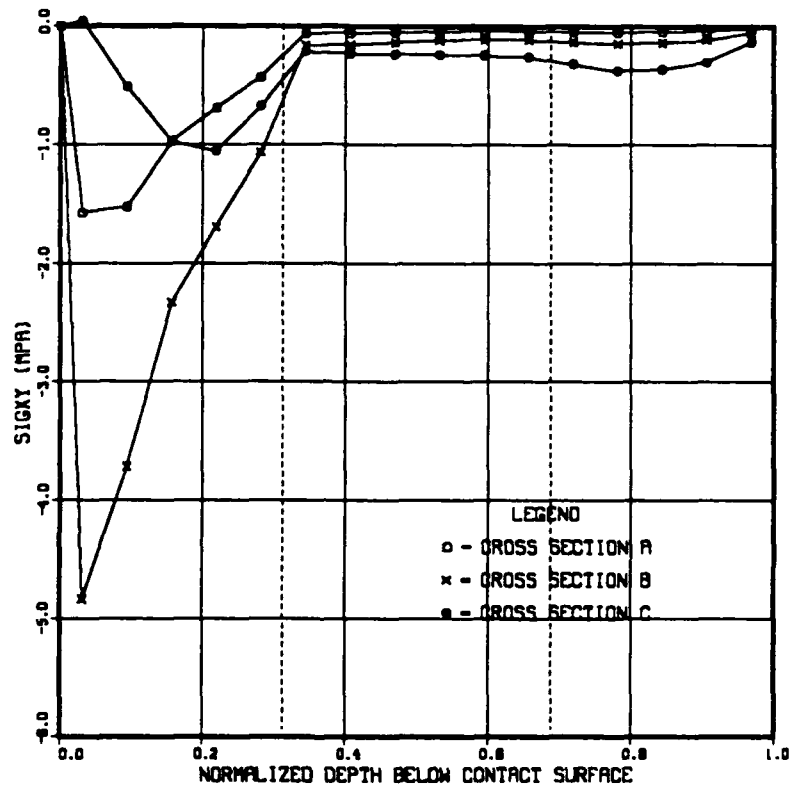


Figure 35. Stress distribution: τ_{xy} for 0(5)-ISO(6)-0(5) laminate

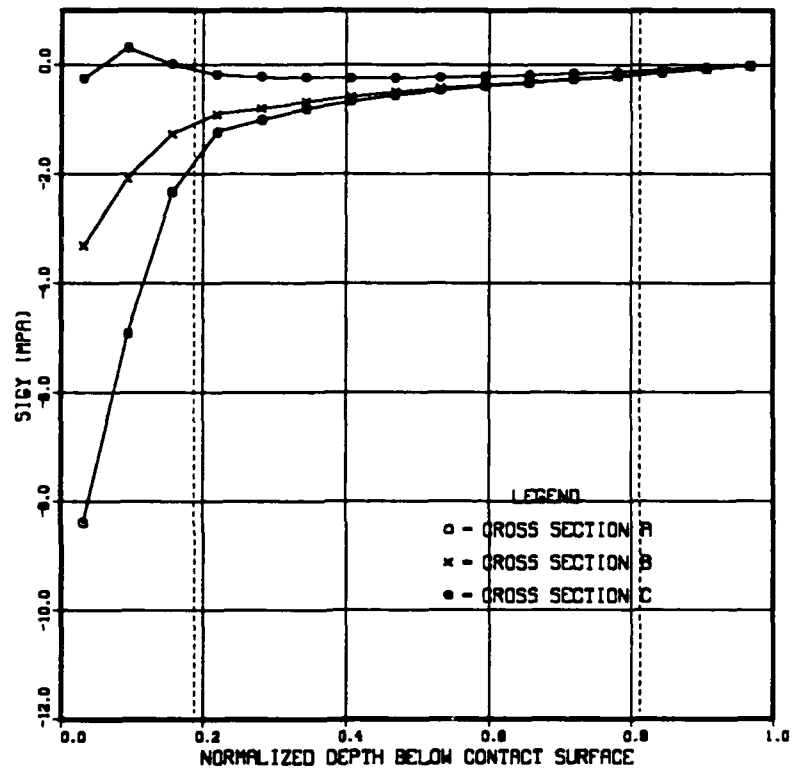


Figure 36. Stress distribution: σ_y for 0(3)-ISO(10)-0(3) laminate

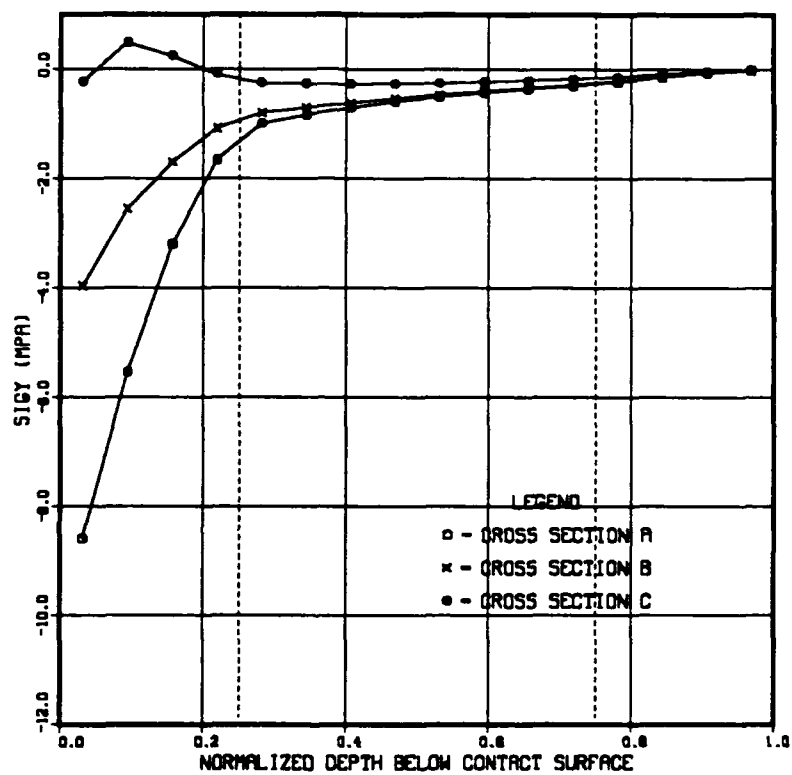


Figure 37. Stress distribution: σ_y for 0(4)-ISO(8)-0(4) laminate

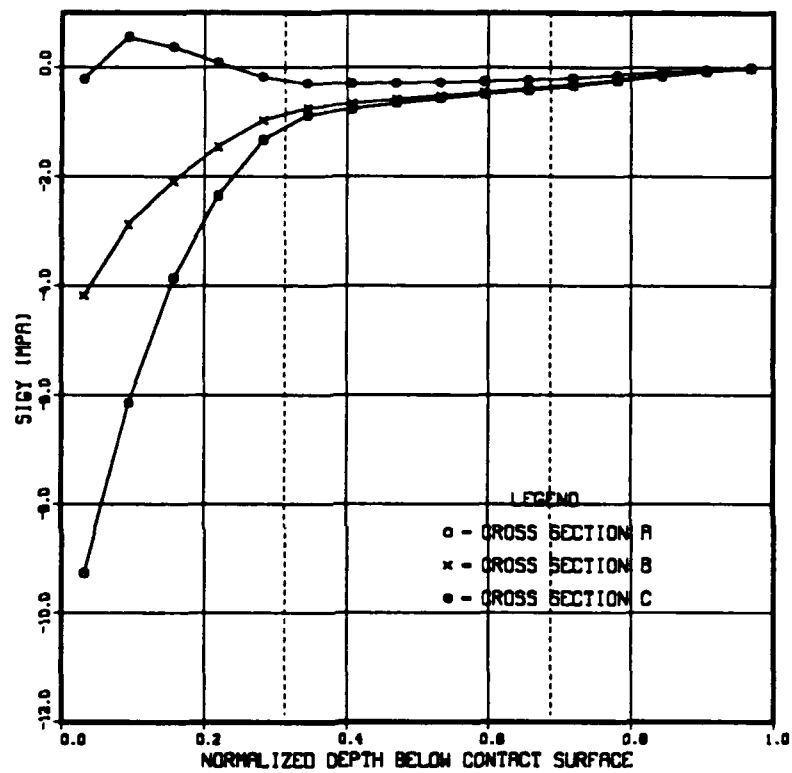


Figure 38. Stress distribution: σ_y for 0(5)-ISO(6)-0(5) laminate

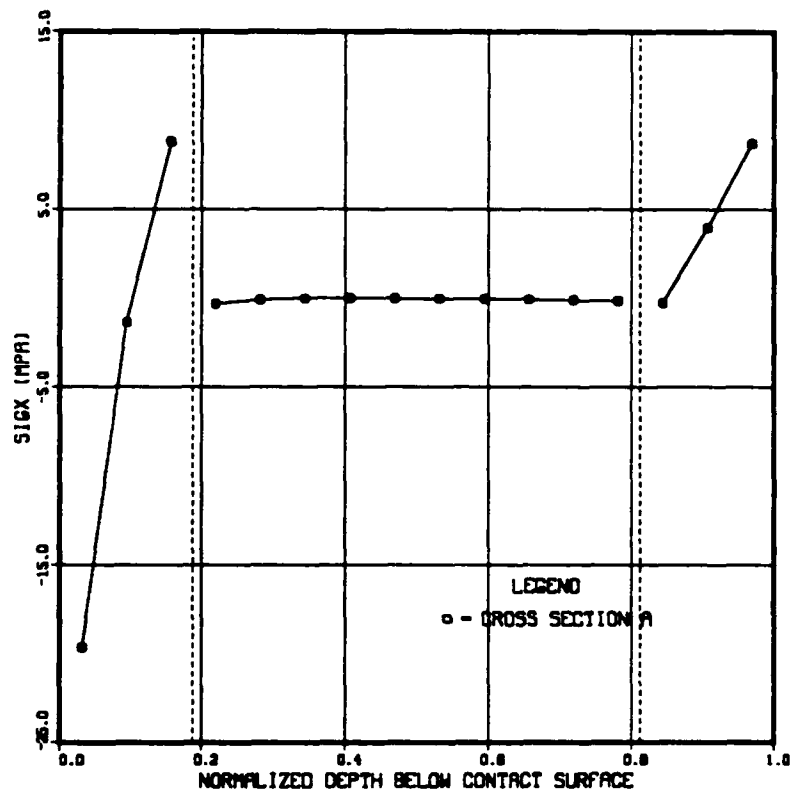


Figure 39. Stress distribution: σ_x for 0(3)-ISO(10)-0(3) laminate

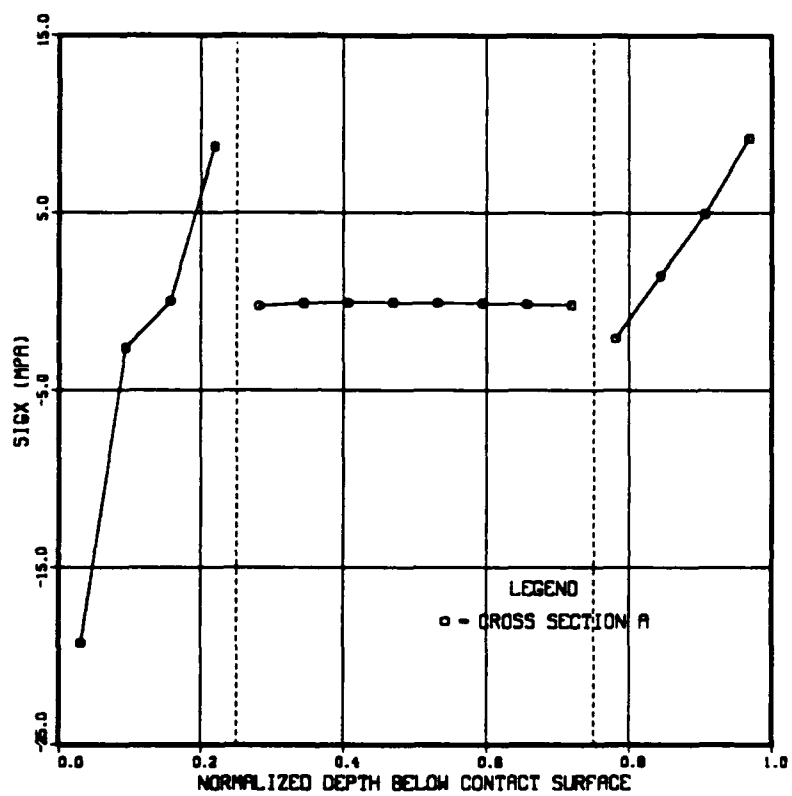


Figure 40. Stress distribution: σ_x for 0(4)-ISO(8)-0(4) laminate

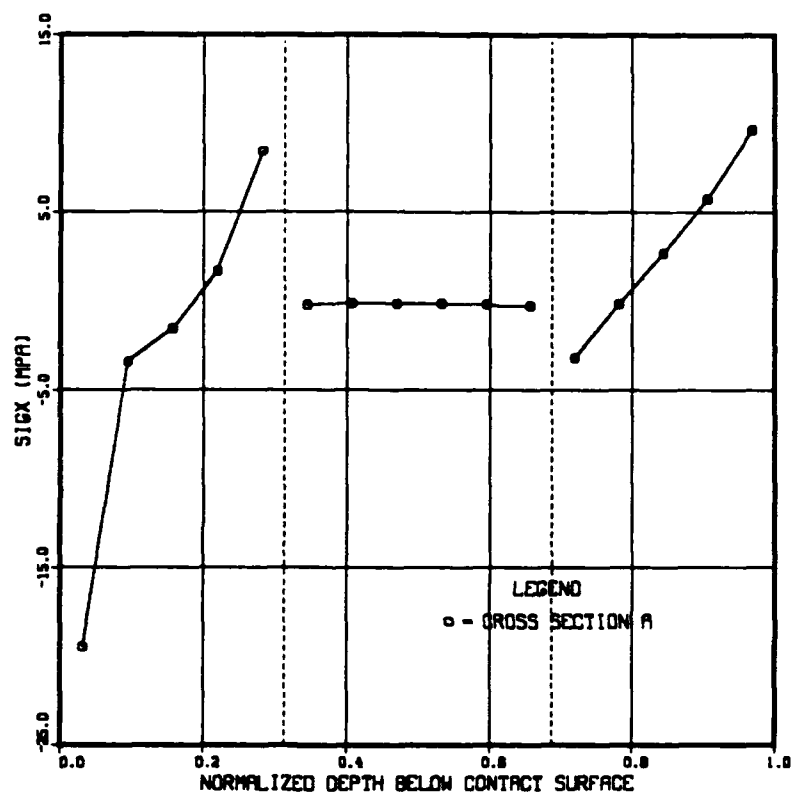


Figure 41. Stress distribution: σ_x for 0(5)-ISO(6)-0(5) laminate

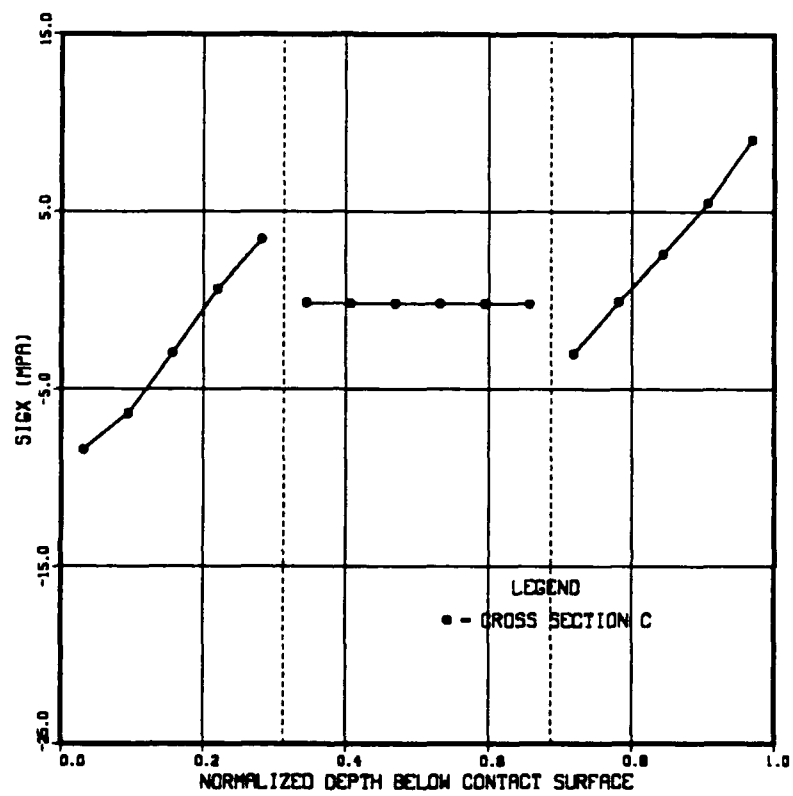


Figure 42. Stress distribution: σ_x for 0(5)-ISO(6)-0(5) laminate at cross section C

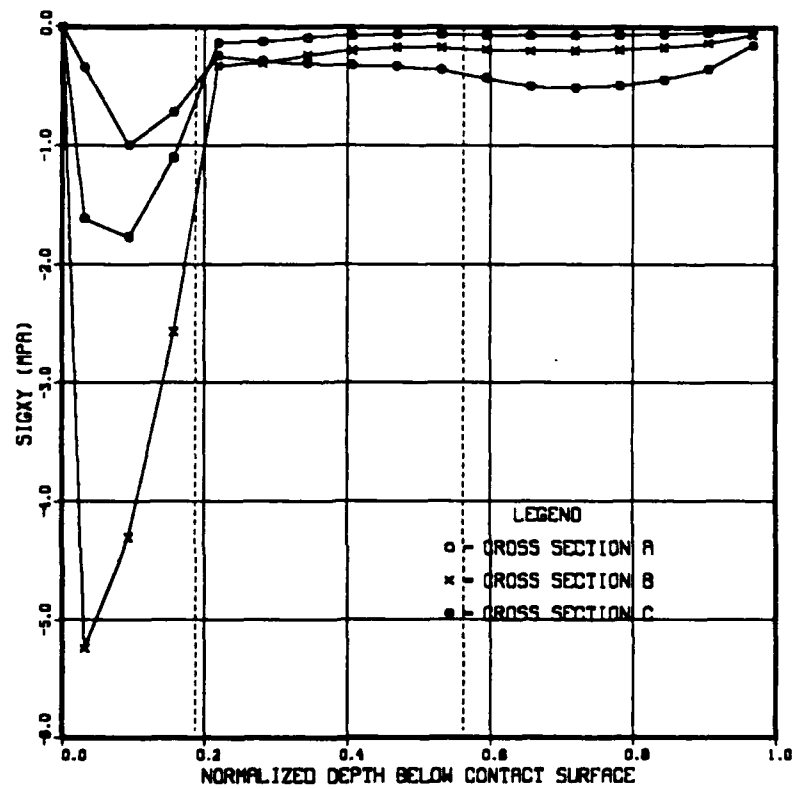


Figure 43. Stress distribution: τ_{xy} for 0(3)-ISO(6)-0(7) laminate

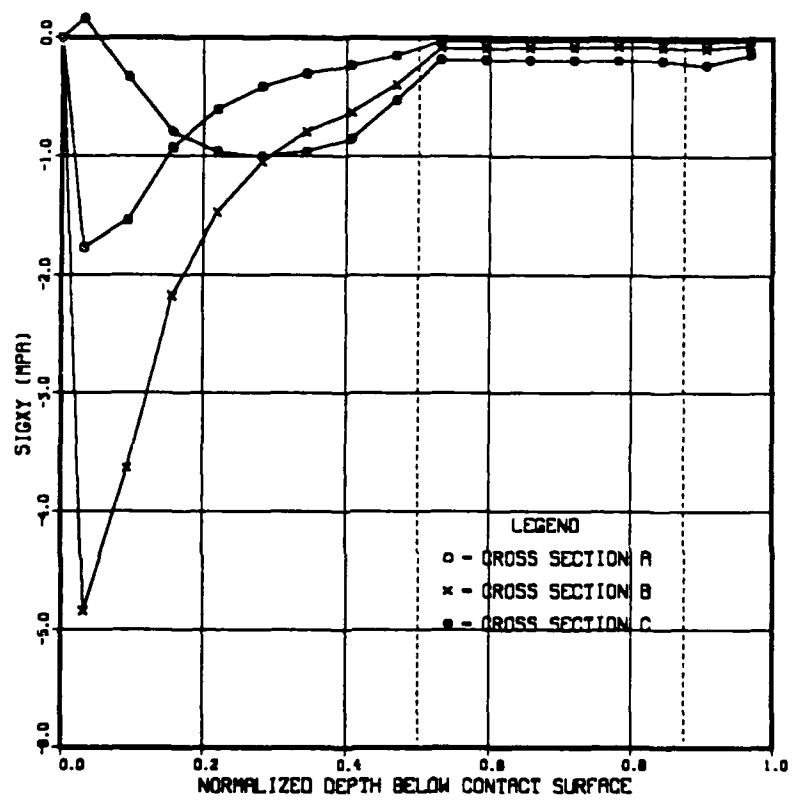


Figure 44. Stress distribution: τ_{xy} for 0(8)-ISO(6)-0(2) laminate

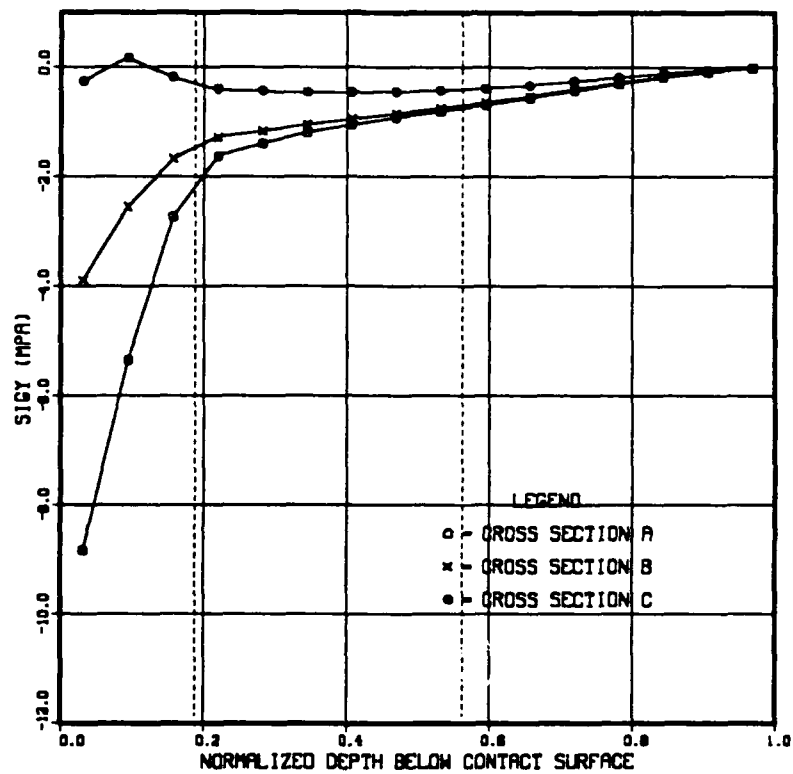


Figure 45. Stress distribution: σ_y for 0(3)-ISO(6)-0(7) laminate

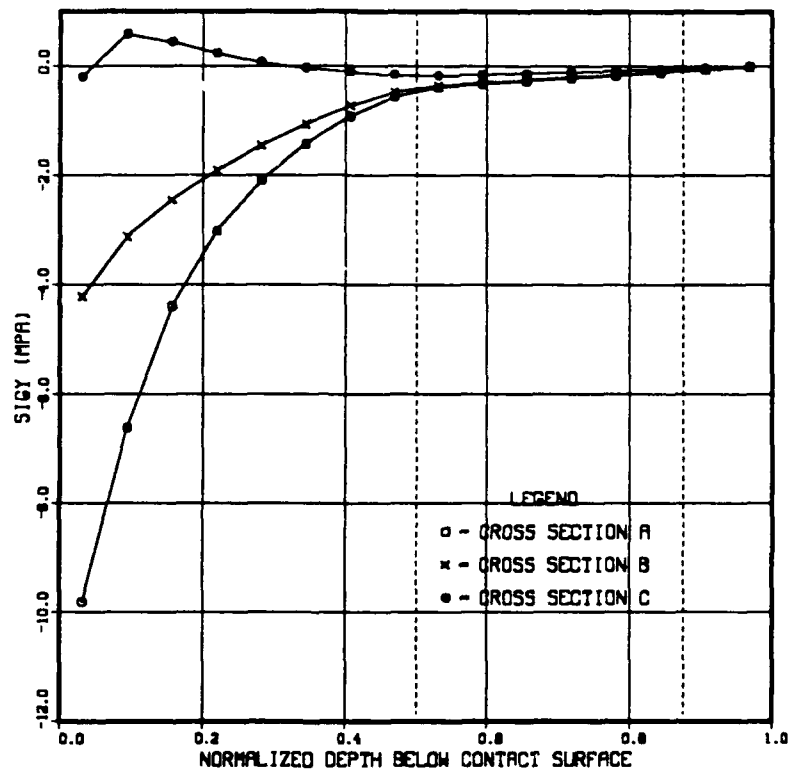


Figure 46. Stress distribution: σ_y for 0(8)-ISO(6)-0(2) laminate

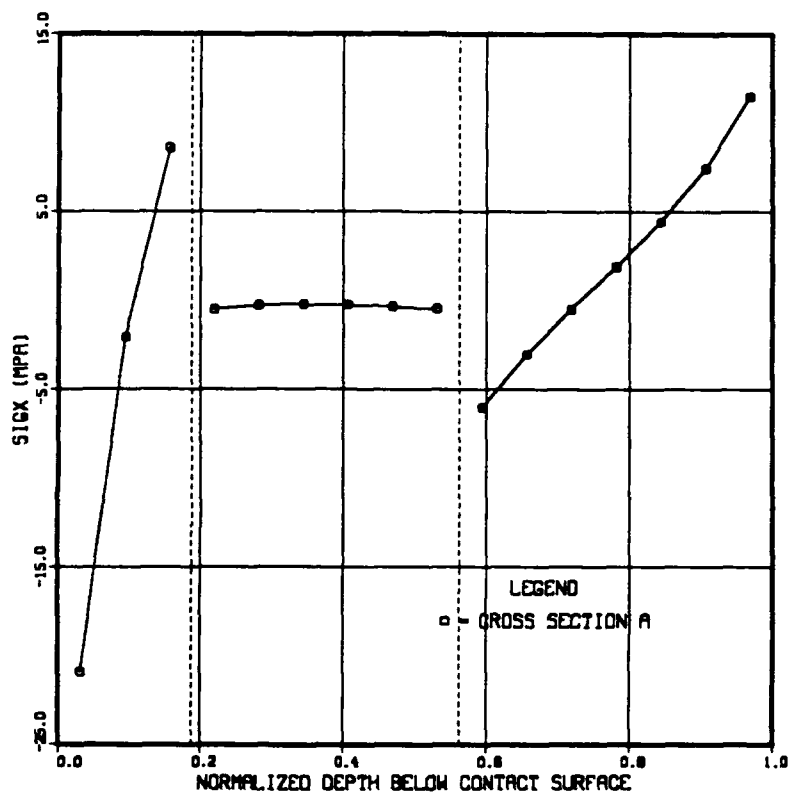


Figure 47. Stress distribution: σ_x for 0(3)-ISO(6)-0(7) laminate

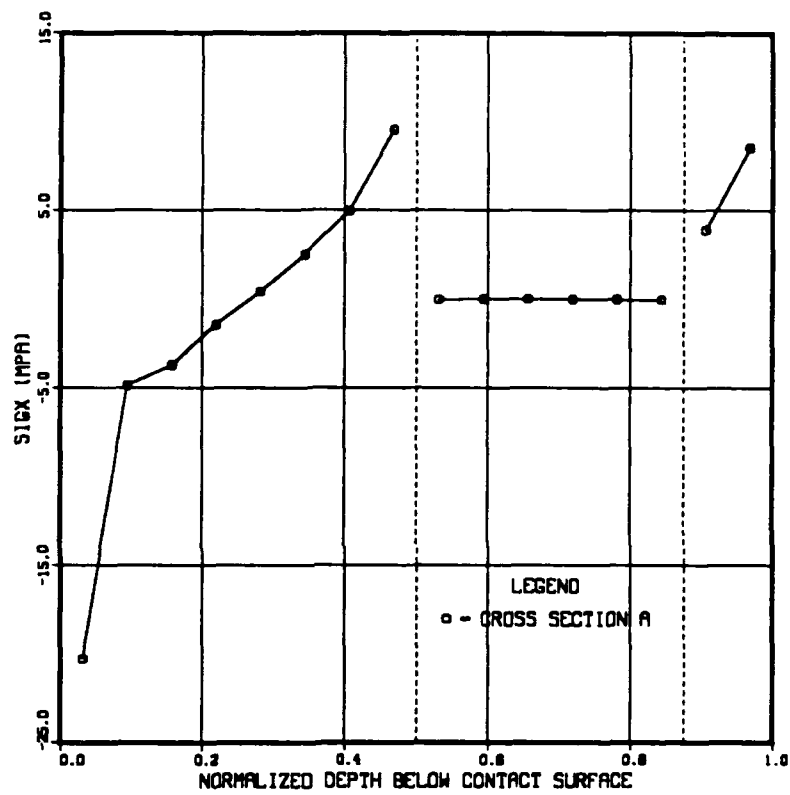


Figure 48. Stress distribution: σ_x for 0(8)-ISO(6)-0(2) laminate

V. CONCLUSIONS AND RECOMMENDATIONS

This study has developed two methods for approximating contact stresses using the augmented Lagrange multiplier method. As illustrated in Part A of Chapter IV, these methods accurately approximate the stresses that result from contact between a cylinder and plane surface. This study has also illustrated how this approach can be applied to understand the behavior of an actual contact problem by examining the response of a composite plate to low velocity impact.

A. RAYLEIGH-RITZ APPROACH

In the process of developing these methods, a number of comments can be made regarding the application of the Rayleigh-Ritz method to solving contact stress problems.

1. The selection of the trial function is an extremely challenging process. If it is desired to determine the deformation in a contact problem, the proper stress field must be first satisfied. Because of this, the selection of possible trial functions is limited. For example, when selecting a trial function for the vertical deformation of the foundation of Figure 1, a suitable selection is given by the following equation:

$$v(x,y) = f(x) \cos\left(\frac{\pi y}{2H}\right)$$

This equation exhibits the favorable characteristics of maximum deformation at the contact surface and diminishing deformation as the distance from the contact surface increases. If contact stresses are to be modeled, this trial function is inappropriate. Calculation of ϵ_y is as follows:

$$\epsilon_y = \frac{\partial v}{\partial y} = -f(x) \frac{\pi}{2H} \sin\left(\frac{\pi y}{2H}\right)$$

This function exhibits zero strain at the point of contact increasing to maximum strain at the lower boundary.

2. Since the selection of trial functions is difficult, the task is further impeded by complicated geometries. Furthermore, selection of a trial function necessitates that some knowledge of the deformation field exists. Without a sensible selection of trial functions, an accurate approximation is unlikely.
3. This method assumes the trial function in the form of an infinite series. Solution accuracy theoretically should improve with an increased number of terms. However, precautions must be taken to ensure the solution is numerically stable as the number of terms increases. Since the strain energy calculations require integration, there are choices of trial functions that will increase without bound as the number of terms is increased. This problem can be controlled by normalizing dimensions or limiting the choice of trial functions.

4. An increase in accuracy was observed as the number of constraints was increased and the distance between consecutive constraints was decreased. It is believed that the improved accuracy results from a better definition of the contact surface.

B. FINITE ELEMENT APPROACH

The results in Chapter III illustrated that this approach of applying the finite element method to contact stress analysis is effective. A number of comments can be made regarding this approach to problem solving.

1. As illustrated in the results, this method accurately approximated the isotropic roller bearing problem. However, some difficulties were encountered during the modeling of the multi-ply composite. In this model, smooth trends of decreasing deformations were often interrupted by spurious deformations or groups of deformations. These interruptions occurred within layers of significantly reduced stiffness. It is believed that the optimization routine had difficulty approximating the deformations through these layers because of their very small contribution to strain energy. As stated in the results, the contact boundary conditions were obtained from the optimization program and applied to a direct finite element program to solve the problem. The above difficulty is recognized as a limitation of this approach.
2. This approach is much more flexible for complicated geometries than the Rayleigh-Ritz approach. In addition, detailed knowledge of the deformation field is not needed as required by the Rayleigh-Ritz approach.
3. The application of static condensation is crucial to the successful implementation of this method. Every effort should be made to reduce the number of design variables to improve optimization efficiency.

C. COMMENTS ON OPTIMIZATION

A number of observations were made regarding the general use of the Automated Design Synthesis System and the specific usage of the augmented Lagrange multiplier method.

1. The global optimum was more likely to be determined when the objective function was normalized.
2. For both the Rayleigh-Ritz approach and the finite element approach, the initial choice of design variables had a significant affect on the possibility of obtaining the global optimum. For the Rayleigh-Ritz method, initial selections of design variables can result in largely dissimilar values of strain energy and external work, the two components of the objective function. It was determined that convergence was more likely when optimization commenced with these two terms on the same order of magnitude. With regard to the finite element approach, sensible choices of the initial design variable vector was necessary for convergence to the global optimum. This was accomplished by intuitive selection of design variables to model the likely deformation.
3. Solution accuracy can be improved by scaling constraint equations. It has been stated that in some circumstances, some constraints change more rapidly than

others and can influence the solution excessively while others have little influence [Ref. 6: p. 136].

4. With regard to the usage of the augmented Lagrange multiplier method, it was frequently necessary to 'tune' the optimization algorithm to a specific problem. This was done by varying the initial penalty term p and the initial Lagrange multiplier term λ . As stated by Vanderplaats, commencing optimization with a small value of p should theoretically suffice for most problems [Ref. 6: pp. 137-138]. However, it was frequently necessary to select an initial value for p due to convergence to unrealistic solutions. Similarly, an initial choice of the Lagrange multiplier term can effect the solution. Commencement with a small value is again recommended. [Ref. 6: p. 141]. This need to 'tune' the problem is a significant drawback to using this optimization method. The ideal way to overcome this limitation is to first tune the optimization routine using a known solution. With this accomplished, this approach can be used for meaningful data collection.

D. SANDWICH COMPOSITE MATERIAL STUDY

The behavior of sandwich composite materials to low velocity impact loading was successfully investigated by the application of the finite element approach. A number of observations can be made from examining the results.

1. The maximum shear stress is relatively insensitive to layer thicknesses. However, as the thickness of the contact layer increases, a reduction of the interface shear stress is observed.
2. Tensile transverse normal stresses exist at some cross sections away from the contact zone. However, this stress is always compressive at the interface. Compressive transverse stresses increase in beams with smaller cores due to reduced deflection and contact zone size.
3. As the thickness of the layer closest to the contact zone increases, a nonlinear distribution of bending stress within this layer intensifies. This phenomenon is localized to the region of contact.
4. As the thickness of the layer opposite to the contact zone increases, bending crack propagation toward the core is less likely due to increased compressive bending stresses within the layer.

E. RECOMMENDATIONS FOR FURTHER STUDY

The methods developed in this study offer a basis from which additional research can grow. A reasonable direction is the relaxation of some of the assumptions made in Chapter II Part B. For example, relaxation of the rigid roller assumption and the frictionless surface assumption would provide challenging research. Models with complex geometry could be created. For example, a model of a pin loaded bolt connection could be created with rigid or non-rigid pins. Implementation of these changes would provide a versatile and highly applicable model for contact stress analysis.

REFERENCES

1. Pian, T. H. H., and Kubomura, K., "Formulation of Contact Problems by Assumed Stress Hybrid Elements," pp. 49-59: Wunderlich, W., et.al., Eds., *Nonlinear Finite Element Analysis in Structural Mechanics: Proceedings of the Europe-U.S. Workshop*, Ruhr-Universität at Bochum, Germany, July 28-31, 1980. Berlin, Springer, 1981.
2. Cheng, W. Q., Zhu, F. W., and Luo, J. W., "Computational Finite Element Analysis and Optimal Design for Multibody Contact System," *Computer Methods in Applied Mechanics and Engineering*, v. 71, pp. 31-39, November 1986.
3. Nour-Omid, B., and Wriggers, P., "A Two-Level Iteration Method for Solution of Contact Problems," *Computer Methods in Applied Mechanics and Engineering*, v. 54, pp. 131-144, February 1986.
4. Guerra, F. M., and Browning, R. V., "Comparison of Two Slideline Methods Using ADINA," *Computers and Structures*, v. 17, pp. 819-834, June 1983.
5. Bischoff, D., "Indirect Optimization Algorithms for Nonlinear Contact Problems," pp. 533-545: *Conference on the Mathematics of Finite Elements and Applications (5th: 1984: Brunel University)*, London, Academic Press, 1985.
6. Vanderplaats, G. N., *Numerical Optimization Techniques for Engineering Design with Applications*, McGraw-Hill Book Company, 1984.
7. Pierre, D. A., and Lowe, M. J., *Mathematical Programming Via Augmented Lagrangians*, Addison-Wesley Publishing Company, Inc., 1975.
8. Rothert, H., Idelberger, H., Jacobi, W., and Niemann, L., "On Geometrically Nonlinear Contact Problems with Friction," *Computer Methods in Applied Mechanics and Engineering*, v. 51, pp. 149-154, September 1985.
9. Joshi, S. P., and Sun, C. T., "Impact Induced Fracture in a Laminated Composite," *Journal of Composite Materials*, v. 19, pp. 51-66, January 1985.
10. Sun, C. T., and Rechak, S., "Effects of Adhesive Layers on Impact Damage in Composite Laminates," pp. 97-123, *Composite Materials: Testing and Design (Eighth Conference)*, ASTM STP 972, J. D. Whitcomb, Ed., American Society for Testing and Materials, Philadelphia, 1988.
11. Choi, H. Y., Wang, H. S., and Chang, F. K., "Effect of Laminate Configuration and Impactor's Mass on the Initial Impact Damage of Graphite Epoxy Composite Plates due to Line-Loading Impact," *Journal of Composite Materials*, v. 26, No. 6, pp. 804-827, 1992.
12. Ugural, A. C., and Fenster, S. K., *Advanced Strength and Applied Elasticity*, 2d ed., Elsevier Science Publishing Co., Inc., 1987.
13. Shigley, J. E., and Mishke, C. R., *Mechanical Engineering Design*, 5th ed., pp. 71-74, McGraw-Hill Publishing Company, 1989.
14. Burnett, D. S., *Finite Element Analysis from Concept to Applications*, p. 568, Addison-Wesley Publishing Company, 1987.

15. Kwon, Y. W., and Akin, J. E., "Materially Non-Linear Analysis of Body Contact Using a Finite Element Method," *Engineering Computations*, v. 3, pp. 317-322, December 1986.
16. Jones, R. M., *Mechanics of Composite Materials*, pp. 37-41, Hemisphere Publishing Corporation, 1975.
17. Babiloglu, E., *A Numerical Study of Dynamic Crack Propagation in Composites*, Master's Thesis, Naval Postgraduate School, Monterey, California, September 1992.

INITIAL DISTRIBUTION LIST

		No. Copies
1.	Defense Technical Information Center Cameron Station Alexandria, VA 22304-6145	2
2.	Library, Code 52 Naval Postgraduate School Monterey, CA 93943-5002	2
3.	Department Chairman, Code ME Department of Mechanical Engineering Naval Postgraduate School Monterey, CA 93943-5000	1
4.	Naval Engineering Curricular Office, Code 34 Department of Mechanical Engineering Naval Postgraduate School Monterey, CA 93943-5000	1
5.	Professor Young W. Kwon Department of Mechanical Engineering Naval Postgraduate School Monterey, CA 93943-5000	2
6.	Dr. Rembert F. Jones, Jr. Submarine Structures Division Code 172, Bldg 19, Room A236B Naval Surface Warfare Center, Carderock Division Bethesda, Maryland 20884-5000	1
7.	Lieutenant Eric S. McDonald, USN Route 2 Box 174 Kenbridge, VA 23944	1